Bottom-Up Fabrication of a Metal Supported Oxo-Metal Porphyrin

D. A. Duncan[1,2]*, P. S. Deimel[1], A. Wiengarten[1], M. Paszkiewicz[1], P. Casado Aguilar[1‡], R. G. Acres[3¶], F. Klappenberger[1], W. Auwärter[1], A. P. Seitsonen[4,5], J. V. Barth[1] and F. Allegretti[1]*

[1] Physics Department E20, Technical University of Munich, D-85748 Garching, Germany
[2] Diamond Light Source, Harwell Science and Innovation Campus, Didcot, OX11 0QX, United Kingdom
[3] Elettra-Sincrotrone Trieste S.C.p.A., S.S. 14-km 163.5, 34149 Basovizza, Trieste, Italy
[4] Département de Chimie, École Normale Supérieure, 24 rue Lhomond, F-75005 Paris, France
[5] Université de recherche Paris-Sciences-et-Lettres, Sorbonne Université, Centre National de la Recherche Scientifique, F-75005 Paris, France

* Email: francesco.allegretti@ph.tum.de; david.duncan@diamond.ac.uk

‡ Present address: Instituto Madrileño de Estudios Avanzados en Nanociencia, Cantoblanco 28049, Madrid, Spain

¶ Present address: Australian Synchrotron, 800 Blackburn Road, Clayton, Victoria, 3168, Australia

Abstract

In situ **preparation of oxotitanium tetraphenylporphyrin (TiO-TPP) on Ag(111) under ultra-high vacuum conditions was achieved in a multi-step procedure starting from adsorbed free-base tetraphenylporphyrin (2H-TPP). The final product as well as the intermediate titanium tetraphenylporphyrin (Ti-TPP) were characterized by a suite of surface-sensitive spectroscopic tools combined with scanning tunneling microscopy and density functional theory (DFT), and compared against the parent 2H-TPP species. Facile oxidation of Ti-TPP with molecular oxygen was observed at 300 K, with X-ray photoelectron spectroscopy (XPS), and near-edge X-ray absorption fine structure (NEXAFS) from the Ti 2*p* core levels supporting a change in the oxidation state from Ti^{2+} to Ti^{4+}. N *K*-edge and Ti *L*-edge NEXAFS suggest that the tetrapyrrole macrocycle conformation is modified upon binding to oxygen, in agreement with DFT calculations that predict a marked change of the local environment of the Ti centers upon oxygen attachment. O *K*-edge NEXAFS and O 1*s* energy-scanned photoelectron diffraction from the resulting TiO-TPP monolayer provide strong evidence for the presence of a titanium-oxygen double bond, with the latter technique yielding a bond length of 1.56 ± 0.02 Å. The majority of adsorbed TiO-TPP species have the oxo group pointing away from the surface rather than towards it, and thus the oxygen atom can potentially interact with external species. Both the highly reactive, intermediate Ti-TPP species and the final product TiO-TPP are of great interest for catalytic applications.**

Introduction

The study of metal-organic complexes supported on solid substrates is a highly dynamic field of research, stimulated by the promise of these compounds for applications in, e.g., future electronics[1-5], molecular catalysis[6-10], dye-sensitized solar cells[11-12] and biomedical technology[13-14]. Within this field, porphyrins and phthalocyanines, two important tetrapyrrole compounds, are among the most studied classes of molecules due to the robustness and ease of synthesis, and the wide range of functionalities[15-16]. Indeed, the ability to coordinate different metal ions into the center of their

macrocycle can be exploited to impart a variety of electronic and chemical properties, which can be further tailored by the choice of peripheral substituents attached to the macrocycle. In view of practical applications, a first important issue is how the interaction with supporting substrates modifies the functional properties of the adsorbed molecules. Furthermore, for applications in catalysis, photocatalysis, gas transport and gas sensing devices the formation of oxo-metal species is of tremendous importance. It will be, for almost any redox reaction, a necessary intermediate state and, in an oxidizing environment, will almost certainly be the ground state for many metalloporphyrins. More specifically, when in solution, the oxoiron[17], oxoruthenium[18] and oxomanganese[19-20] porphyrins are, themselves, active for catalysis and oxygen transfer. Imparting the reactivity and gas transport properties of these molecules into a solid state system (i.e. supporting these molecular species on solid substrates) can thus be crucial for "heterogenizing" these homogeneous catalysts, and for providing metal electrode contacts for gas sensing and gas transport applications.

However, recent work by our group on the reactivity of different metal centers in tetraphenylporphyrin (Figure 1a) immobilized on Ag(111)[9] demonstrated that the presence of the noble metal substrate appears to attenuate their reactivity. In particular, there is evidence of a total suppression of the reactivity of ruthenium tetraphenylporphyrin (Ru-TPP) towards dioxygen, a muted reactivity of manganese tetraphenylporphyrin (Mn-TPP)[21], but still a strong reactivity of titanium tetraphenylporphyrin (Ti-TPP – shown schematically inFigure 1Figure 1b). From this work, we evince that, if one wants to utilize this molecular class supported on a metallic substrate for applications akin to those in solution, then metalloporphyrins that interact more strongly with external molecular species need to be utilized. As such, we believe that Ti-TPP could be an interesting model system for probing the reactivity of substrate-anchored metalloporphyrins. Furthermore, oxotitanium porphyrins have been theoretically predicted to be able to photocatalytically split water into $H^{\bullet}$ and $OH^{\bullet}$ radicals utilizing two visible photons[22]. In accordance with this prediction, in 2014, Morawski *et al*. experimentally verified that micro-crystallites of oxotitanium tetraphenylporphyrin species on fused silica plates, dipped into an aqueous solution of NaOH and terephthalic acid, produce $OH^{\bullet}$ radicals when illuminated by light with a wavelength of 445 nm (~2.8 eV) and 570 nm (~2.2 eV)[23].

Within this background, we present here a recipe for creating titanium (Ti-TPP – Figure 1b) and oxotitanium tetraphenylporphyrin (TiO-TPP – Figure 1c) *in situ* in ultra-high vacuum (UHV), as well as we illustrate an in-depth characterization of the chemical, electronic and structural properties of the resulting adsorbate species. The fine control provided by this bottom up approach to the fabrication of adsorbed Ti- / TiO-TPP monolayers will facilitate fundamental studies into the reactivity of these species anchored on metallic substrates.

Experimental

a. Experimental Methods and Computational Details

XPS (X-ray photoelectron spectroscopy), SXPS (XPS with soft X-ray synchrotron light), UPS (ultraviolet photoelectron spectroscopy), PhD (energy-scanned photoelectron diffraction), NEXAFS (near-edge X-ray absorption fine structure), and STM (scanning tunneling microscopy) measurements were performed on TPP species adsorbed on Ag(111) single crystals from the Surface Preparation Laboratory.

The XPS measurements were performed on a custom-built ultra-high vacuum (UHV) chamber usually mounted at the Technical University of Munich (TUM) and operating at a base pressure of 5×10^{-11} mbar. Here, the X-rays come from a polychromatic Al *Kα* source (main photon line at 1486.6 eV) and the photoemitted electrons are detected with a SPECS PHOIBOS 100 CCD analyzer. For the PhD and

O *K*-edge NEXAFS measurements, the same chamber was connected to the UE56-2-PGM-2 beam line at the BESSY-II storage ring in Berlin to exploit X-ray radiation of tunable energy. The O *K*-edge NEXAFS data were acquired by using the hemispherical analyzer in constant final state mode (detection of a fixed kinetic energy and summation of the signal over all detector channels), recording the O *KVV* Auger intensity while varying the incident photon energy from 520 to 555 eV.

SXPS, Ti $L_{2,3}$-edge and N *K*-edge NEXAFS measurements were performed at the permanent end-station of the Materials Science beam line on a bending magnet at the ELETTRA light source (Trieste, Italy). This end-station is equipped with a SPECS PHOIBOS 150 hemispherical electron energy analyzer. The NEXAFS data were acquired by monitoring decay electrons within a 30 eV kinetic energy window covering the Ti $L_{2,3}M_{2,3}M_{2,3}$ and N *KVV* transitions, respectively; at a generic photon energy much above the absorption edges these transitions overlap, in principle, in the kinetic energy region around 380 eV[24-25], but in practice, at the two respective edges only one is found to be appreciably excited.

To minimize possible effects from radiation damage during the longer absorption measurements, the photon flux was appropriately reduced, and relevant core levels were monitored by SXPS between two successive NEXAFS scans to rule out degradation of the layers during the acquisition time. In addition, the sample was moved laterally before recording a new spectrum. However, particular considerations apply to the O 1*s* core-level spectra, as discussed below.

STM measurements were carried out in a custom designed UHV system equipped with a CreaTec low temperature STM (LT-STM). For all measurements the sample was held at 6 K and the system base pressure was below 5×10^{-10} mbar. The STM images were acquired in constant current mode and with the bias applied to the sample.

All above-mentioned UHV chambers were equipped with standard facilities for ion sputtering (Ar or Ne gas) and sample heating, home-built evaporators for the deposition of 2H-TPP and the Ti metal, and leak valves for O_2 dosing. A clean Ag(111) surface was prepared by sputtering at room temperature (RT), followed by annealing to 725 K.

The N *K*-edge and Ti *L*-edge NEXAFS data were – in the first step – normalized by the drain current from a gold mesh that was located at the last valve separating the experimental chamber from the Materials Science beam line. This drain current is assumed to be proportional to the flux of the incident light. From the normalized data, a similarly processed spectrum measured on the clean Ag(111) surface was subtracted. Prior to subtraction, this "clean" spectrum has been normalized to share the same pre-edge intensity as the corresponding NEXAFS spectrum. Finally, the resulting subtracted spectra were normalized to the intensity of the post-resonance region, such that the intensity of the absorption edge is approximately 1. The O *K*-edge NEXAFS spectra that have been recorded at BESSY-II were processed in a similar manner. The data were normalized by the drain current from the last mirror of the beam line and a similarly normalized "clean" / O-free spectrum, which was acquired by measuring the O *KVV* Auger region of a densely packed 2H-TPP monolayer on Ag(111).

XPS and SXPS signals were fitted using a Gaussian line shape due to the widths of the peaks being significantly greater than the associated lifetime broadening. Inelastic losses were fitted using a Gaussian error function that shared the same energy and width as the Gaussian line shape, and the background was fitted with a straight line. The displayed XPS and SXPS data thus have had both the error function and the straight line subtracted. The energy scale of the individual spectra was corrected *via* subsequent measurements of the Ag $3d_{5/2}$ (binding energy 368.27 eV)[26-27] core level at the same photon energy. The quoted angles of the NEXAFS spectra, θ, relate to the angle between the photon polarization and the surface normal following the conventional notation.

The O 1*s* energy-scanned photoelectron diffraction (PhD)[28-29] measurements on TiO-TPP/Ag(111) were performed by acquiring the O 1*s* core level (within a binding energy region of 523 to 534 eV) over a photon energy range of 630 to 874 eV. For the main O 1*s* signal, this corresponds to a kinetic energy range of approximately 100 to 344 eV. In order to compensate for the background in the O 1*s* PhD spectra, the same PhD measurement was performed on a densely packed 2H-TPP monolayer on Ag(111). This measurement was used as a template background, simply multiplied with a straight line to match the data, and served to remove the strong underlying Ag Auger features. In order to obtain the area under the O 1*s* photoemission peaks, these were modeled by a Voigt line shape, which was exploited to gain a more accurate measure of the relative photoelectron intensity. The calculated area was then plotted as a function of the peak kinetic energy, and a stiff spline was subsequently fitted through the data, which was subtracted from and used to normalize the peak area and provide the characteristic photoelectron diffraction modulations, $\chi(E_{kin})$, in the photoemission intensity as a function of kinetic energy (and therefore photon energy). To extract the structural information contained in such modulations, the χ-curves were modeled using the Fritzsche multiple scattering code described elsewhere[30-35], exploiting the front end developed by the Diamond Light Source. The fit was performed by only considering the scattering from the TiO-TPP molecule itself (including substrate Ag atoms in high symmetry sites below the Ti metal centers in the scattering made no significant difference to the quality of fit). A Particle Swarm Optimisation[36] was used to rapidly explore the variable hyperspace.

The STM images were processed in WSxM[37] with row-by-row subtraction of a parabola before high pass filtering by fast Fourier transform to remove periodic background noise.

Simulations of the Ti *L*-edge absorption spectra were performed using the CTM4XAS code (version 5.5) of F. M. F. de Groot and E. Stavitski[38], which incorporates both crystal-field and charge-transfer effects. For the two metal complexes studied in this work, Ti-TPP and TiO-TPP, the D_{4h} symmetry (square planar or distorted octahedral) was chosen, following previous work on porphyrins and phthalocyanines[39-40]. In the O_h symmetry (octahedral), the 3*d* orbitals are split into t_{2g} (d_{xy}, d_{xz}, d_{yz}) and e_g (d_{z^2}, $d_{x^2-y^2}$) sublevels with energy difference 10 *Dq*. When the symmetry is lowered from O_h to a tetragonally distorted D_{4h}, the energy levels are split further into e_g (d_{xz}, d_{yz}), b_{2g} (d_{xy}), b_{1g} ($d_{x^2-y^2}$), and a_{1g} (d_{z^2}), such that two additional parameters need to be introduced, *Dt* and *Ds*. Accordingly, in the simulations the crystal-field parameters 10 *Dq*, *Dt* und *Ds* were adjusted to reproduce the distinctive features of the experimental *L*-edge absorption spectra. As allowed by the CTM4XAS program, the calculated spectra were broadened with Lorentzian (full width at half maximum, FWHM: 0.2 eV) and Gaussian (FWHM: 0.4 eV) functions, describing the lifetime and instrumental broadening, respectively. Three additional parameters, the Slater integral reduction factors F_{dd}, F_{pd} and G_{pd}, were also given as input for the simulations.

Density functional theory (DFT) calculations were performed by means of the Quantum ESPRESSO package[41]. We used the vdW-DF2-B86r approximation[42] in the exchange-correlation term, and considered five layers of the substrate, whereby the three outermost layers were allowed to relax relative to the bulk-terminated positions. An optimized lattice constant of 4.1325 Å, 2×2 *k* points, Fermi-Dirac smearing of occupation numbers with a 50 meV broadening, projector augmented wave (PAW)[43] data sets for the pseudisation of the core electrons, surface-dipole corrections and cut-off energy of 60 Ry for the wave functions and 350 Ry for the electron density were utilized. A rectangular unit cell (20.3×20.1 Å^2) with a two-point basis was used. The separation between the two neighboring molecules in the basis was 14.3 Å, in good agreement with the experimental values (14.0 – 14.2 Å) for TPP species[44-45].

b. Preparation of a TiO-TPP monolayer

A densely packed TiO-TPP monolayer was prepared in five sequential steps. In the first step, a multilayer of 2H-TPP (Sigma Aldrich, >99% purity) was evaporated onto the clean Ag(111) crystal from a quartz glass crucible kept at 550 K. The 2H-TPP powder was purified *in situ* by degassing it for prolonged time at the evaporation temperature. In the second step, excess 2H-TPP was removed by annealing the sample at 500 K for 15 minutes, leaving a characteristic 2H-TPP monolayer on the Ag(111) surface[46-47]. The 2H-TPP molecules were then metalated *in situ* in UHV, following an established methodology[48-49], by evaporating Ti from a resistively heated Ti-W filament, a homemade stranded wire consisting of interwoven single titanium and tungsten wires. The thickness of the evaporated Ti was monitored by a quartz crystal microbalance at known distance from the Ti-W wire, and a $1/r^2$ relationship was assumed for scaling the thickness deposited onto the surface. As the metalation proceeded only partially at room temperature, the sample was subsequently annealed to 500 K in order to achieve completion. To shorten the preparation time, it turned out that the preceding four preparation steps could be reduced to evaporating both 2H-TPP and Ti, subsequently, with the Ag(111) sample held at 500 K. In the last preparation step, the Ti-TPP was exposed to ~100-200 L of O_2 gas (purity grade 5.0, from MESSER) with the sample held at RT. Note that, for the presented STM measurements, a sub-monolayer coverage of TiO-TPP was prepared in order to provide areas of clean Ag(111) surface to form the STM tips. Moreover, in this STM investigation the Ti coverage was intentionally kept lower than that necessary for full metalation, in order to contrast the different appearance of free-base and metalated species.

Results

2H-TPP

2H-TPP on Ag(111) has been thoroughly studied in recent years (cf. Refs. [15-16] and references therein) and the results obtained in this work are in agreement with the literature. Nevertheless, for the sake of completeness and in order to aid the comparison with Ti- and TiO-TPP, these results on 2H-TPP are briefly described here.

The N 1*s* SXP spectra of 2H-TPP (e.g. Refs. [46-47, 50-52]) contain two well-separated peaks at a binding energy of 398.1 and 400.1 eV (Figure 2a), corresponding to the two chemically inequivalent N species in the molecule (Figure 1a). As the two chemical species appear in a 1:1 ratio, both peaks are of comparable intensity. The N *K*-edge NEXAFS spectra (Figure 2b; cf. also Refs. [51-52]) contain three clearly distinct features in the pre-edge region, which are presumably due to overlapping transitions arising from the excitation of electrons from the two different initial N 1*s* states into non-degenerate π* states (the lowest unoccupied molecular orbital, LUMO, and higher-lying states)[53]. The near complete dichroism between the grazing (θ = 10°) and normal incidence (θ = 90°) geometries (Figure 2b) indicates that the tetrapyrrole macrocycle adsorbs flat on the surface.

UPS measurements show a HOMO (highest occupied molecular orbital) state centered at ~1.9 eV and a HOMO-1 state at ~3.1 eV binding energy. The latter manifests as a shoulder on the valence band of the Ag substrate (Figure 3a, red curve).

In STM images (Figure 4a with 2H-TPP contours highlighted in dark blue; cf. also Refs. [46, 54-55]) at negative bias of -1.0 V (tunneling from the surface into the tip), the center of the 2H-TPP molecules shows a diamond-like shape which is assigned to the tetrapyrrole macrocycle. The four outer lobes are assigned to the tilted phenyl rings. The phenyl rings of neighboring molecules orientate in a T-shape[16, 21, 56]. At a positive bias of 0.5 V (tunneling from the tip into the surface) a two-fold shape becomes

evident (Figure 4b and Refs. [55, 57-58]) for the macrocycle, usually attributed to the so-called "saddle-shape" of the molecule [44, 55, 57, 59]. Moreover, 2H-TPP forms well-ordered islands with a square unit cell and a specific azimuthal orientation of the molecules relative to the underlying substrate[54].

Ti-TPP

The metalation of 2H-TPP with titanium can be clearly observed in the N 1*s* SXP spectrum with synchrotron radiation of Figure 2c. Upon incorporation of the Ti atom into the macrocycle the inequality of the two N species is lifted, accompanied by the displacement of the two central hydrogen atoms which leave the system as H_2 (e.g., Ref.[60]). The Ti 2*p* XP spectrum recorded with Al *Kα* (Figure 5a – adapted from Ref.[9]) is particularly broad, and the Ti $2p_{3/2}$ component at lower binding energy clearly contains a main feature around 455.8 eV and a broad shoulder extending up to 459.0 eV. In the curve-fitting analysis, both the $2p_{3/2}$ and $2p_{1/2}$ core levels are thus separated into a major line and a satellite feature. When comparing the peak areas of the N 1*s* and Ti 2*p* XP spectra acquired in the TUM UHV chamber with Al *Kα* radiation (see Figure S1 in the supporting information, SI), and correcting for the relative photoemission cross-sections at 1486.6 eV, a ratio of 4.1±0.4 : 1 is found, confirming that all Ti on the surface has been incorporated into the TPP molecules, and subsequent annealing to higher temperatures results in no observable differences in the N 1*s* core level.

In apparent contrast to the Ti 2*p* XP spectrum of Figure 5a, where both core-level lines show a satellite feature, the STM images of Ti-TPP only showed a single shape for the Ti-TPP molecules (Figure 4a, b), with a three lobe structure comparable to that of Fe-TPP[46] and Co-TPP[44] (Figure 4a, molecules outlined in green). Note that these STM images are taken from the same area of the surface as our previously reported STM images[9], but at a different bias (-0.1 V in our prior work). At negative bias (- 1 V), the median lobe of this shape appears at the center of the molecule, while the two, somewhat brighter, outer lobes are apparently located above a pyrrole unit. At positive bias (+0.5 V), the three lobes appear instead with similar brightness, forming a single elongated protrusion. In general, the origin of the outer lobes is not immediately evident, as the molecule would be expected to be fourfold symmetric rather than twofold symmetric. The enhanced tunneling may be due to an overlap of the d_{xz} or d_{yz} orbitals of the Ti atom with surface states of the underlying Ag(111) substrate, however, one might expect these two orbitals to be degenerate*. On the other hand, a twofold symmetric appearance of metallo-tetraphenylporphyrins on threefold symmetric surfaces is not uncommon in the literature and has previously been related to an adsorption-induced distortion of the macrocycle from the planarity of the free (i.e. unsupported) species.[44, 61] Furthermore, in the 2H-TPP islands the metalation seems to be favored along certain directions, apparently leading to chains of metalated molecules that are defined by the alignment of the lobes, possibly indicative of existing intermolecular interactions (see Figure 4c). Note also that the metalation does not lift the order and packing found for the 2H-TPP assembly. In general, it is possible that the higher molecular coverage or the higher Ti coverage used in the XPS and SXPS experiments could result in the presence of more than just one chemically distinct Ti-TPP species, however, as 2H-TPP exhibits island growth and the Ti metalation does not alter the molecular arrangement inside the islands, such a coverage effect is not expected.

Thus, based on the evidence collected from the STM data, the origin of the broad shoulders toward higher binding energy in the Ti 2*p* XP spectra (Figure 5a) is ascribed to a final state effect in the photoemission rather than to the presence of Ti-TPP species in a different chemical state. In particular, we speculate that it arises from multiplet splitting. Nominally, in the absence of major charge transfer occurring from or to the substrate, the Ti ion in Ti-TPP should be in a 2+ state. The binding energy

* This expectation is largely borne out in the modelling of the Ti *L*-edge NEXAFS and the Ti-TPP projected DOS (cf. Figures S8 and S9 of the SI).

position (455.8 eV) of the major Ti $2p_{3/2}$ component on Ag(111) would be consistent with this case, as substantiated in Ref. [9] on the basis of available literature[62]; this leaves potentially two unpaired electrons in the valence shell ([Ar]$3d^2$).[63-65] Hence, the broadness of the Ti 2*p* XPS could be evidence of the coupling between the angular momentum of the partly filled core shell left behind upon photoemission and the angular momenta of the electrons in the valence shell yielding a multiplicity of states.[66] Such an effect was indeed predicted for Ti^{2+} in Ref. [67], however experimental evidence is missing in the literature, due to the difficult access to systems with exclusively Ti^{2+} ions. Final-state-effect satellites were reported for TiN[68-69] and generally attributed to *shake-up* processes, whereby the latter term was used to distinguish between additionally observed plasmon losses and losses associated to the coupling between core and valence electrons.

The N *K*-edge NEXAFS spectrum corresponding to the partly metalated system of Figure 2c is shown in Figure 2d. The analogous SXP and NEXAFS spectra for a fully metalated layer are shown in Figure S2 in the SI. The *K*-edge NEXAFS spectra indicate that the incorporation of Ti induces a moderate decrease of the dichroism, and thus an increase in the average tilt of the pyrrole rings of the macrocycle (Figure 2d). However, NEXAFS cannot distinguish whether this is due to an increase in the size of the proposed saddle shape conformation[44, 55, 57, 59] or to the macrocycle reforming into a square pyramidal shape. Although the twofold nature of the STM image discussed above may be compatible with a saddle shape distortion, it is also possible that the difference in contrast in the STM images is due to electronic, rather than geometric, effects. Beyond the change to the dichroism in the N *K*-edge NEXAFS, the spectrum for Ti-TPP now consists of only two clear features (cf. Figure 2d and Figure S2 in the SI). This reflects the reduction of the initial N 1*s* core level from two states (corresponding to the two chemically inequivalent nitrogen atoms in 2H-TPP) to one, which is presumably being excited into two non-degenerate π^* orbitals.

The Ti $L_{2,3}$-edge NEXAFS spectrum at θ = 90° (Figure 5b, the pertaining Ti 2*p* SXP spectrum is shown in the left panel of Figure S3) shows two features per spin-orbit component, which are not clearly resolved at θ = 10°. The splitting between these two features is about 2 eV, thus appreciably smaller than the binding energy difference (> 3 eV) between the two spectral features we find when fitting the Ti $2p_{3/2}$ line of Figure 5a. In addition, the relative intensity of these two features in the NEXAFS is reversed with respect to that expected if they arose from different initial states corresponding – hypothetically – to the two features identified in the respective XP spectrum. In fact, the weaker feature in XPS occurs at a higher binding energy and thus should actually appear at higher photon energy in the NEXAFS spectrum. Hence, as the splitting of the two distinct features in each spin-orbit component in the NEXAFS does not correspond to the two features seen in XPS, this evidence further supports the broad XPS Ti 2*p* lines being caused by final state effects rather than by the presence of different chemical states. Indeed, due to the different final states populated by resonant excitation (NEXAFS) and photoelectron emission (XPS), final-state effects can contribute in a markedly different way to the measured intensity in the two cases. Specifically, the two features per spin-orbit component in the NEXAFS can presumably be attributed to the splitting between t_{2g} and e_g sub-levels of Ti and are distinctive of the specific coordination of the Ti atom and the crystal field in its surrounding.

As the L_3-edge spectra of rutile and anatase TiO_2 present a sharp and narrow t_{2g} band (centered at about ~458 eV) and a clearly split e_g band at higher energy (centered at ~460-461 eV)[40, 70-72] due to distortion of the octahedral coordination environment[73-74], it is inferred that in the case of Figure 5b the Ti atoms are not embedded in their rutile or anatase configuration. However, NEXAFS is not only sensitive to the symmetry of the coordination environment of the Ti atoms but also depends crucially on the oxidation state of the latter and the occupation of the 3*d* shell. In this sense, the measured spectra and especially the one recorded with out-of-plane polarization (black curve in Figure 5b) bear a strong resemblance with the ELNES (energy loss near-edge structure) spectrum of cubic TiO in Ref.[71],

where the octahedrally coordinated Ti^{2+} ions give rise to two broad spectral features at about 457.5 (L_3) and 462.5 eV (L_2), respectively. A rather similar spectral appearance, albeit with a slight shift to higher energy, is also reported for the NEXAFS $L_{2,3}$-edge of TiO in Ref.[75]. The close resemblance to the published data thus suggests that NEXAFS may enable the formal oxidation state of the central Ti ion in the molecules to be determined in a more conclusive way than allowed by XPS, as will be substantiated below.

The UPS measurements of Ti-TPP (Figure 3a) display little change in the shape and position of the HOMO and HOMO-1 features. However, metalation induces occupation of additional states near the Fermi edge, at ~0.4 eV, which could be the origin of the very bright lobe structure of the negatively biased STM image of Figure 4a. Similar spectral features located ~ 1 – 1.5 eV above the HOMO of the parent 2H-TPP were previously observed for other metalloporphyrins in valence band studies by both UPS and STS (scanning tunneling spectroscopy)[44, 47, 51, 76] and DFT calculations[44, 77]. Albeit with different conclusions regarding the degree of hybridization with the underlying substrates[44, 51, 76], these features were invariably related to the *d* levels of the central ions. In the case of Ti-TPP therefore, the observed increase of density of states could be indicative of the chemical state of the Ti atoms, which is nominally 2+ and therefore still retains two electrons in the outer 3*d* shell. While the possibility of a static charge transfer from the Ag substrate into the former LUMO of the molecule[78-79] cannot be entirely disregarded, it is important to note that the Ti-TPP species seem to interact attractively, as evidenced by the preference to form chains rather than isolated species. This is quite unlike the case of porphine on Ag(111)[79], where a similar proposed charge transfer results in clear repulsion between adjacent molecules.

TiO-TPP

Exposure of the Ti-TPP monolayer to 100-200 L O_2 at RT results in a significant sharpening and a pronounced shift to higher binding energy of the spin-orbit components in the Ti 2*p* XP spectrum (Figure 5c – adapted from Ref.[9]). In addition, two separate features become apparent in the O 1*s* SXPS (Figure 6), whereas in the O *K*-edge NEXAFS two sharp resonances are seen (Figure 7). Of the two species in the O 1*s* SXP spectrum, the one at higher binding energy was found to be highly beam-sensitive, whereas the other was observed to be very stable, suggesting that the individual components do indeed arise from two chemically distinct species, rather than a potential energy loss (or shake-up) mechanism. In the O *K*-edge NEXAFS, the two resonances display a clearly opposing dichroism between the two geometries with out-of-plane (θ = 7°) and largely in-plane (θ = 60°) polarization, respectively. It is possible, in principle, that these two resonances arise from the two different chemical species on the surface, indicating that one oxygen species binds perpendicular to the surface, the other parallel. However, the O 1s SXPS shows that the coverage of the beam-sensitive species is far less than that of the beam-stable species, whereas the two resonances in the O *K*-edge NEXAFS are of comparable intensity. Thus, we rather assign both resonances to originate from the same initial state and, instead, assign the lower photon energy resonance at 529.5 eV to excitation into a π^* state and the resonance at 530.5 eV to excitation into a σ^* state. The σ^* transition is surprisingly sharp, which would indicate that both the π^* and σ^* state lie below or at the vacuum level, and are thus bound states. Such assignment agrees well with the interpretation given for titanyl phthalocyanine on Ag(111) in Ref.[80].

Hence, the O *K*-edge data in conjunction with the Ti 2*p* XPS strongly suggest the formation of a TiO moiety with the oxygen atom forming a double bond to the Ti atom. From the observed linear dichroism in the NEXAFS it is inferred that this oxo group is mainly oriented perpendicular to the surface; the O atom must either point away from or toward the surface. To determine the exact

orientation of the Ti–O bond (at least for the predominant, beam-stable species) O 1*s* energy-scanned photoelectron diffraction (PhD) measurements were performed. For the beam-stable component in the O 1s SXPS (Figure 6, red), very strong modulations (± 40%) were observed (Figure 8, red solid line) and found to be very similar in periodicity, though almost twice as intense, to those of the O 1*s* PhD of vanadyl phthalocyanine[81]. The beam-sensitive feature was found to have practically no measurable modulations (Figure 8, green dotted line), though it is important to note that the markedly weaker intensity of this feature in the core-level spectra and the progressive beam damage result in a significantly higher noise level and lower reliability of the PhD modulation. From a qualitative level, this suggests that the beam-stable species creates a TiO moiety with the oxygen atom further above the surface than the titanium atom, such that strong backscattering from the Ti atom is expected. The data would also support the idea that the beam-sensitive species has the oxygen closer to the surface than the titanium atom, assuming that this species has a variable registry with respect to the underlying substrate[45] that average out diffraction effects. A quantitative analysis of the O 1*s* PhD modulations, following a similar procedure as in the work of Duncan *et al*.,[81] was pursued for the beam-stable species and resulted in an excellent agreement between the theoretical multiple scattering calculations and the experimental data (Figure 9). The best fit, R = 0.04 (variance of 0.02), was found for the O atom directly atop the Ti atom (lateral displacement: 0.0 ± 0.3 Å) at a height of 1.56 ± 0.02 Å ($d_{Ti\text{-}O}$). Although a single experimental geometry is a comparatively small data set on which to base a geometric structure, as is seen in the work on vanadyl phthalocyanine[81] inverting the orientation of the molecule has a dramatic effect on the expected photoelectron diffraction modulations. Therefore, we conclude that the O atom must be directed away from the surface for the majority of adsorbed TiO-TPP on Ag(111), as in the case of a titanyl phthalocyanine monolayer on the same surface[82].

The oxidation to TiO-TPP causes no change in the N 1*s* SXPS (Figure 2e), with the binding energy associated to the Ti-N coordination remaining at 398.6 eV (cf. also Table S1). Conversely, the N *K*-edge NEXAFS data (Figure 2f) indicate that the oxidation of Ti-TPP to TiO-TPP induces a third final state at higher photon energies. The origin of this new state is not immediately clear, however, it does imply that the coordination of the oxygen atom has an influence on the nitrogen atoms of the macrocycle and the unoccupied electronic states of the molecule. At a first glance it is notable that the N *K*-edge NEXAFS shows a larger effect due to the coordination of O to the Ti atom, than the corresponding N 1*s* SXPS. However, it is not surprising, considering that the N 1*s* core level is localized solely on the N atoms, whereas the unoccupied valence band orbitals that are being excited into at the N *K*-edge NEXAFS are presumably delocalized over the whole molecule. Thus, while the coordination of oxygen has an apparent effect on the binding energy of the unoccupied molecular orbitals, it does not affect appreciably the electron density at the N atom, exerting little to no effect on the N 1*s* binding energy. At any rate, the decreased residual signal in the π*-state NEXAFS region at θ = 90° signals a slightly flatter conformation of the macrocycle compared to Ti-TPP.

The Ti *L*-edge NEXAFS spectra (Figure 5d, the pertaining Ti 2*p* SXP spectrum is shown in the right panel of Figure S3) are markedly different from those of Ti-TPP above (Figure 5b), with a more clearly discernible fine structure and generally sharper features. Specifically, in the spectrum excited with in-plane polarization (θ = 90°), the splitting between the (presumably) t_{2g} band and the center of the e_g sub-levels in the L_3- and L_2-edges amounts to about 3.0 – 3.2 eV and, contrary to the observation for Ti-TPP, the e_g band exhibits a clear splitting of around 1.2 eV (cf. L_3-edge at θ = 10°, out-of-plane polarization). This may suggest that the Ti ion is now coordinated in a more octahedral – albeit strongly distorted – configuration, reminiscent of the coordination in the rutile or anatase structures[70, 73-74]. For TiO-TPP, this coordination can be interpreted to arise from the tetradentate macrocycle and the two out-of-plane ligands, the latter consisting of the oxygen atom and – as shown in Ref.[83] – the underlying Ag(111) substrate.

In the STM experiments, in spite of the presence of a large fraction of non-metalated molecules (see contrast in Figure 4c), after exposure to 100 L O_2 most of the species on the surface look strikingly similar (Figure 4d). Indeed, the contrast in STM of TiO-TPP is reminiscent of that of 2H-TPP (cf. white and dark blue outlines in Figure 4d, highlighting TiO-TPP and 2H-TPP species, respectively), although subtle differences emerge as a function of bias (Figure 4e). Inspection of Figure 4 indicates, on the one hand, a distinct modification of the appearance of the metalated (Ti-TPP) species upon exposure to oxygen. On the other hand, the similarity in contrast between TiO-TPP and 2H-TPP, especially at negative biases, most likely indicates that states localized on the TiO moiety are not involved in the tunneling process and that the HOMO level is dominated by the TPP core. Thus, the TiO-TPP species can be differentiated from 2H-TPP and Ti-TPP in STM, however, small differences in appearance between individual TiO-TPP molecules are observed. Interestingly, the STM tip would occasionally pick up an unknown species (possibly a CO or water molecule, or an O atom displaced from a TiO-TPP), here generously referred to as "special tip conditions", resulting in a more dramatic difference in contrast between coexisting 2H-TPP and TiO-TPP (see Figure S4 of the SI).

Finally, the exposure to O_2 also causes changes to the valence band spectrum in UPS (Figure 3a). Most notably, the energy state just below the Fermi edge detected for Ti-TPP is clearly quenched, in agreement with both the reduction in contrast of the STM images and the observed similarity to 2H-TPP. Presumably, this quenching is related to the removal of the two outer electrons from the 3*d* shell of the Ti atom. Moreover, the HOMO feature at a binding energy of ~1.9 eV appears slightly weakened in intensity and "softened" in its shape.

DFT calculations

In order to complement the experimental findings, we carried out DFT calculations of the adsorption conformation and electronic structure of adsorbed Ti-TPP before and after coordination of oxygen. Both molecules in the rectangular unit cell (see computational details) were found to adopt a very similar adsorption conformation; however, the Ti centers turned out to be located close to the hcp and fcc hollow sites, respectively, in both cases clearly displaced by ~0.35 Å from the high symmetry site. In Ti-TPP two of the pyrrole rings are clearly bent downward, namely with the N lying below the average plane of the macrocycle and pointing toward the surface, whereas the other two are bent slightly upward. Importantly, the central Ti ion lies drastically below the macrocycle plane by 0.5 – 0.6 Å. This macrocycle conformation, which markedly deviates from the perfect planarity, is thus compatible with the N K-edge NEXAFS data described above. When oxygen coordinates to Ti, the latter atom is pushed dramatically upwards, moving to about 0.6 Å above the macrocycle (as a consequence, its average height above the Ag surface layer increases from 2.7 Å to 4.0 Å). Moreover, the tetrapyrrole macrocycle becomes slightly flatter, with the height difference between the pairs of inequivalent N atoms being reduced from 0.15 to 0.10 Å in good agreement with the N *K*-edge NEXAFS fingerprint of TiO-TPP. The theory also predicts a nearly vertical Ti–O bond that matches the experimental data, whereas the predicted Ti–O bond length (1.63 Å) is slightly overestimated but still in fair agreement with the PhD analysis (1.56 ± 0.02 Å). A schematic of the predicted structures of Ti-TPP and TiO-TPP, highlighting the adsorption height of the Ti atoms and the Ti-O bond length, is shown in Figure 10.

The DFT calculations were also used to determine the occupied density of states (DOS) (Figure 3b, Figure S5) and compare it to the measured UPS data (Figure 3a). In Figure 3b, where the difference with the DOS of Ag(111) is reported, we can indeed observe similar trends as in the experiment, most notably the quenching of the occupied energy state closest to the Fermi level. In general, there is a tendency for the predicted energy features in DFT to be closer to the Fermi energy than in the experiment. This is, however, to be expected due to the use of the GGA-level approximation in the

exchange-correlation term, and it is not affected by the inclusion of the non-local van der Waals-treatment in the correlation term.

Discussion

The results presented in the previous section exemplify the sequential multi-step procedure for preparing a TiO-TPP monolayer on Ag(111) *in vacuo*. We have extensively characterized the parent 2H-TPP species, the intermediate Ti-TPP, and the final product TiO-TPP by using a combination of XPS, UPS, NEXAFS, PhD and STM. It is clear that the obtained TiO-TPP monolayer shares the same ordering as the corresponding, densely packed 2H-TPP layer and the intermediate Ti-TPP layer it is grown from. However, the intermediate Ti-TPP layer appears to preferentially metalate in chains on the surface, which might indicate some degree of intermolecular interaction within the layer. Upon exposure to molecular oxygen, the Ti-TPP species are readily oxidized. Accordingly, distinct changes can be observed in the Ti 2*p* XPS and Ti *L*-edge NEXAFS signatures as well as in the valence band UP spectrum. Notably, such changes are consistent with an increase in the oxidation state of the Ti ions and the depletion of the outer 3*d* shell. In particular, the XPS binding energy of the Ti $2p_{3/2}$ component of TiO-TPP (457.8 eV, similar to Ref. [82]) and the disappearance of the final-state effects observed for Ti-TPP are suggestive of Ti^{4+} ($3d^0$), as previously pointed out in Ref. [9]. The O 1*s* core level in SXPS shows the presence of two chemically distinct species, a minority species (which is progressively affected by photon exposure) and a majority species (which appears to be more robust under the photon beam). The latter was probed by O 1*s* PhD, and the diffraction data indicate a Ti-O bond length of 1.56 ± 0.02 Å. This bond length is shorter than that obtained for vanadyl phthalocyanine on Au(111) (1.60 ± 0.04 Å)[81], as well as those found in the crystal structures of oxotitanium octaethyl porphyrin (1.613 ± 0.005 Å)[84] and titanyl phthalocyanine (1.650 ± 0.004 Å / 1.626 ± 0.007 Å in different crystal structures)[85]. The DFT calculations also predict a slightly more elongated Ti–O bond (1.63 Å). Nevertheless, the PhD analysis is consistent with an oxygen-titanium double bond, and such a conclusion is corroborated by the presence of both π^* and σ^* resonances in the O *K*-edge NEXAFS spectra. The opposite linear dichroism of the π^* and σ^* components, moreover, shows that the Ti=O bonds are predominantly oriented perpendicular to the surface, whereas the strong photoelectron diffraction modulation in the emission direction perpendicular to the Ag(111) surface clearly indicates that, at least for the majority of adsorbed TiO-TPP molecules, the oxygen atom points away from the surface. This orientation of the TiO moiety is at the origin of the strong backscattering that the O 1*s* photoelectrons experience by the Ti atoms located directly below the O emitter, thus leading to the very large PhD modulation in Figures 8, 9. In addition, the N *K*-edge NEXAFS data suggest that upon binding of oxygen in the TiO-TPP, the tetrapyrrole macrocycle becomes slightly flatter compared to the parent Ti-TPP, in agreement with the DFT predictions. In particular, Ti-TPP exhibits a slightly more pronounced average tilt of the pyrrole rings, which can either be attributed to a saddle shape deformation or to a sort of square pyramidal configuration. The former conformation is indeed more likely, as it is suggested by the DFT analysis and compatible with the pronounced twofold STM appearance.

Regarding the evolution of Ti-TPP into TiO-TPP, a key issue is the oxidation state of the central Ti ions in the adsorbed Ti-TPP and TiO-TPP molecules. XPS is often used for this assignment, and the data reported here suggest that the (formal) oxidation state is increased from 2+ to 4+ from the former to the latter. However, such an assignment based solely on the binding energy position is not unambiguous, due to the appreciable interaction of the molecules with the underlying metal surface and the perturbing effect of the latter on the polarization screening of the 2*p* core holes. Therefore, to address this issue in a more conclusive manner, we turn to the Ti *L*-edge spectra, which not only are sensitive to the structural coordination environment of the Ti ions, but also depend crucially on the occupation of the outer *d* shell. Specifically, we performed simulations of the absorption spectra using

the CTM4XAS code, and the main results are presented in Figure 11 for the best agreement obtained between experimental spectra and simulations at in-plane polarization. In particular, the distinct absorption structures and energy splitting in the TiO-TPP spectrum could only be well-reproduced for a Ti^{4+} ($3d^0$) ion, using the crystal-field parameters 10 *Dq* = 2.35 eV, *Dt* = 0.11 eV and *Ds* = -0.42 eV and Slater integral factors F_{dd} = 1.0, F_{pd} = 0.77 and G_{pd} = 0.75. Interestingly, the optimized values are remarkably similar to those listed in Ref.[40] for a customized titanyl phthalocyanine species with *tert*-butyl peripheral ligands. The agreement not only validates the consistency of the approach but also highlights the dominant role of the tetrapyrrolic coordination of the TiO moiety in determining the *L*-edge absorption signature. Furthermore, the best match to the Ti-TPP spectrum was obtained (as shown in the top part of Figure 11) for a Ti^{2+} ion ($3d^2$) using 10 *Dq* = 2.35 eV, *Dt* = 0.37 eV and *Ds* = +0.67 eV. Thus, only the *Dt* and *Ds* parameters were changed relative to TiO-TPP, the large positive value for *Ds* being now in good agreement with the case of other planar metalloporphyrins and metallophthalocyanines (i.e., without axial ligand).[39] Note that in this case, the values $F_{dd} = F_{pd} = G_{pd} =$ 1.0 were selected to better reproduce the L_2 to L_3 intensity ratio (although this choice does not affect appreciably the spectroscopic signatures), and an energy shift of +2.2 eV was applied. To justify that this energy shift is not arbitrary, the spectrum for Ti^{2+} ions in O_h symmetry was calculated (10 *Dq* = 2.2 eV) and compared with the experimental spectrum of TiO (Ti^{2+}, cubic) of Ref.[71], thus finding a comparable shift of ~2.0 eV to be necessary for good agreement. Importantly, the absorption spectra were also calculated in two other polarizations (namely, out-of-plane polarization and magic angle geometry), as shown in Figures S6, S7. These simulations provide generally good agreement with the experimental data and thus corroborate the final assignment of Ti^{2+} and Ti^{4+} in the Ti-TPP and TiO-TPP species, respectively.

From the crystal-field parameters of the simulations it is possible to calculate the relative energies of the Ti 3*d* manifold for both the Ti-TPP and TiO-TPP species, as displayed in Figure S8. In this simplified one-electron picture, we find that the d_{xy} orbitals (b_{2g}) are significantly stabilized relative to the other *d* orbitals in the TiO-TPP. Such a conclusion is in agreement with previous analysis[40] and confirmed by the DFT-calculated DOS projected on the *d*-orbitals of the Ti atom (PDOS, see Figure S9). The *L*-edge NEXAFS peak just below 456 eV (Figure 11) has therefore strong d_{xy} character. In contrast, the simulations suggest that for Ti-TPP the d_{z^2} orbitals (a_{1g}) are stabilized with respect to the other levels of the manifold and clearly split from the much higher-lying $d_{x^2-y^2}$ orbitals (b_{1g}) by the tetragonal distortion of the complex, as previously argued for metal phthalocyanines[39]. Such a splitting is drastically reduced upon oxidation to TiO-TPP due to the more octahedral-like coordination. Generally, however, the experimental absorption spectra exhibit greater broadening than that predicted by the simulated spectra, which is presumably related to the overlap (not accounted for in the simulations) of, primarily, the d_{z^2} orbitals with the delocalized electrons of the underlying substrate. This overlap may result in the d_{z^2} orbitals, and to a lesser degree the d_{xz} and d_{yz} orbitals, being energetically broadened as is common in hybridized systems[86-87]. The calculated PDOS of Figure S9 shows that such effect is indeed severe in the case of Ti-TPP, in which the Ti atom is much closer (by ~1.3 Å) to the Ag surface compared to TiO-TPP. For this reason, the detailed *d*-level ordering of Ti-TPP extracted within the simplified picture of the CTM4XAS simulations of isolated molecules may not be entirely reliable and indeed the DFT calculations for Ti-TPP/Ag(111) predict the d_{xy} orbitals to lie slightly lower than the d_{z^2}(Figure S9).

Conclusions

In this work we showed that adsorbed TiO-TPP can be prepared on Ag(111) by metalation of free-base 2H-TPP with Ti adatoms followed by exposure to O_2 at RT, and we characterized this promising catalyst

and photocatalyst on the molecular scale by a combination of spectroscopy and microscopy tools. XPS and NEXAFS from the 2*p* core level indicate that the intermediate Ti-TPP has the central Ti ion in a 2+ oxidation state. The presence of two outer electrons in the 3*d* shell is most likely at the origin of the high reactivity of the adsorbed metal complex to O_2, at variance with other supported metalloporphyrins which do not show the same ease of splitting molecular oxygen under UHV conditions[9, 21]. Note that Ti^{2+} complexes are quite uncommon and protecting groups are usually required[88-89], therefore the here prepared Ti-TPP species can also be of high interest for future reactivity studies. When exposing the adsorbed Ti-TPP to dioxygen, the latter is readily split and an oxygen atom binds axially through a double bond to the Ti ion (d_{Ti-O} = 1.56 ± 0.02 Å); the resulting TiO-TPP molecule has the metal ion in a 4+ state and adopts a slightly flatter conformation of the tetrapyrrole macrocycle. Moreover, the majority of adsorbed TiO-TPP molecules have the oxygen atom pointing away from the underlying Ag(111) surface, hence potentially able to coordinate external gas molecules. As proposed in many recent works (e.g. [83, 90-93]), however, the underlying Ag substrate may interact with the metal center in a way that is similar to a ligand bond. The substrate is then expected to play a role, through the molecule-metal coupling, on the reactivity of the TiO moiety. Specifically, the interaction with the underlying substrate is likely to hinder the ability of this molecule to perform photocatalytic reactions due to the rapid quenching of the excited state as observed for copper phthalocyanine on Au(111)[94]. While the TiO moiety could still remain active for purely catalytic reactions, in order to retain the photocatalytic properties it may then be necessary to prepare this species onto a semiconducting or insulating substrate. In this regard, recent studies have discussed the possible formation of titanyl porphyrin species on the rutile TiO_2(110) surface[95-97] and TiO_2 nanoparticles[98].

Supporting Information

Fitted binding energy and FWHM values for the SXPS and XPS spectra shown in the main article (Table S1). Comparison of Ti 2*p* and N 1*s* XP spectra used to determine the N : Ti ratio of a partly metalated Ti-TPP layer (Figure S1). N 1s SXPS and N *K*-edge NEXAFS for a fully metalated Ti-TPP layer (Figure S2). Ti 2*p* SXP spectra corresponding to the measured Ti *L*-edge NEXAFS data of Figure 5 (Figure S3). STM image acquired under "special tip conditions" (Figure S4). DFT-predicted DOS for the three different molecular systems, 2H-TPP, Ti-TPP and TiO-TPP on Ag(111) (Figure S5). Comparison of experimental and simulated Ti *L*-edge NEXAFS spectra in three different photon polarization geometries for TiO-TPP (Figure S6) and Ti-TPP (Figure S7). Energy diagram of the Ti *d*-orbital splitting for Ti-TPP and TiO-TPP (Figure S8) determined from the crystal-field parameters. Projected DOS on the transition metal *d* orbitals calculated by DFT (Figure S9).

Acknowledgements

We are indebted to Prof. Peter Feulner for his assistance during the beam time at BESSY-II and for useful discussion on the measurements. We gratefully acknowledge support given by the staff of the chair E20 at TUM. We also thank Prof. Frank de Groot for valuable advice regarding the CTM4XAS program and Kevin C. Prince for experimental support at the Materials Science beamline. This work was supported by the Deutsche Forschungsgemeinschaft under the Germany's Excellence Strategy (Munich Center for Advanced Photonics and the *e*-conversion Cluster of Excellence EXC 2089/1 – 390776260), the European Research Council Consolidator Grant NanoSurfs (no. 615233), the European Research Council Advanced Grant MolArt (no. 247299), the TUM International Graduate School of Science and Engineering (IGSSE). Financial support for synchrotron beam time was provided by the Helmholtz-Zentrum-Berlin (proposal 15102158-ST) and by the European Community's Seventh

Framework Programme (FP7/2007-2013) under grant agreement number 312284 (CALIPSO project: ELETTRA, proposal 20135344) and is gratefully acknowledged. D.A.D. acknowledges grants from the Alexander von Humboldt Foundation and the Marie Curie Intra-European Fellowship for Career Development (SiliNano, project no. 626397). W.A. acknowledges funding by the Deutsche Forschungsgemeinschaft via a Heisenberg professorship. A.W. acknowledges support by the International Max Planck Research School of Advanced Photon Science (IMPRS-APS). A.P.S acknowledges the computing resources at the Centro Svizzero di Calcolo Scientifico (CSCS), Lugano, Switzerland, under the project uzh11.

Figures:

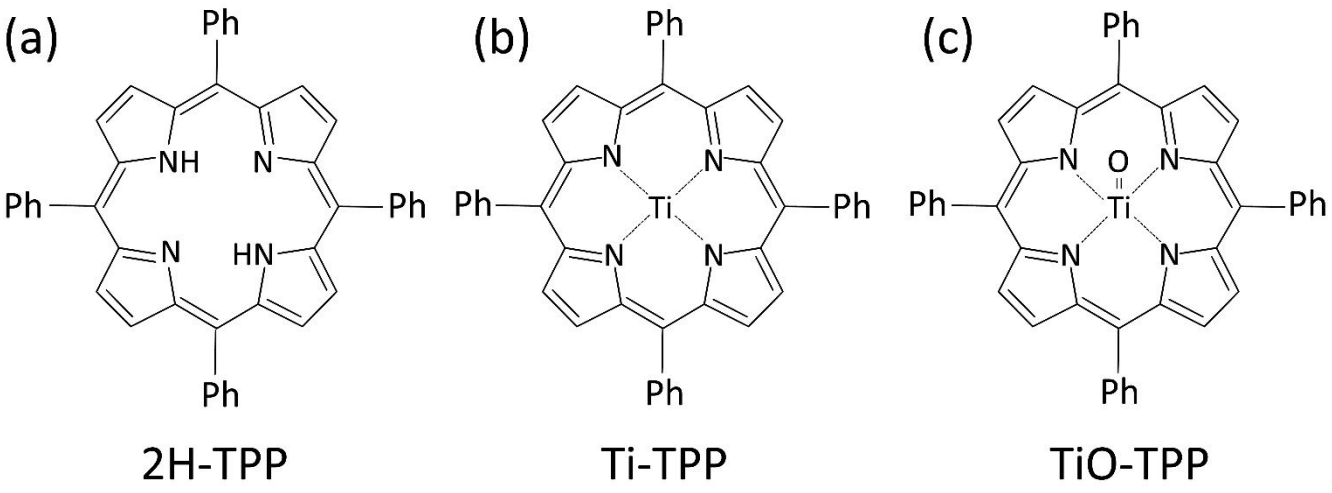

Figure 1: Schematic of (a) free-base tetraphenylporphyrin (2H-TPP), (b) titanium tetraphenylporphyrin (Ti-TPP) and (c) oxotitanium tetraphenyl porphyrin (TiO-TPP). Ph represents a phenyl ring bound at the *meso* position.

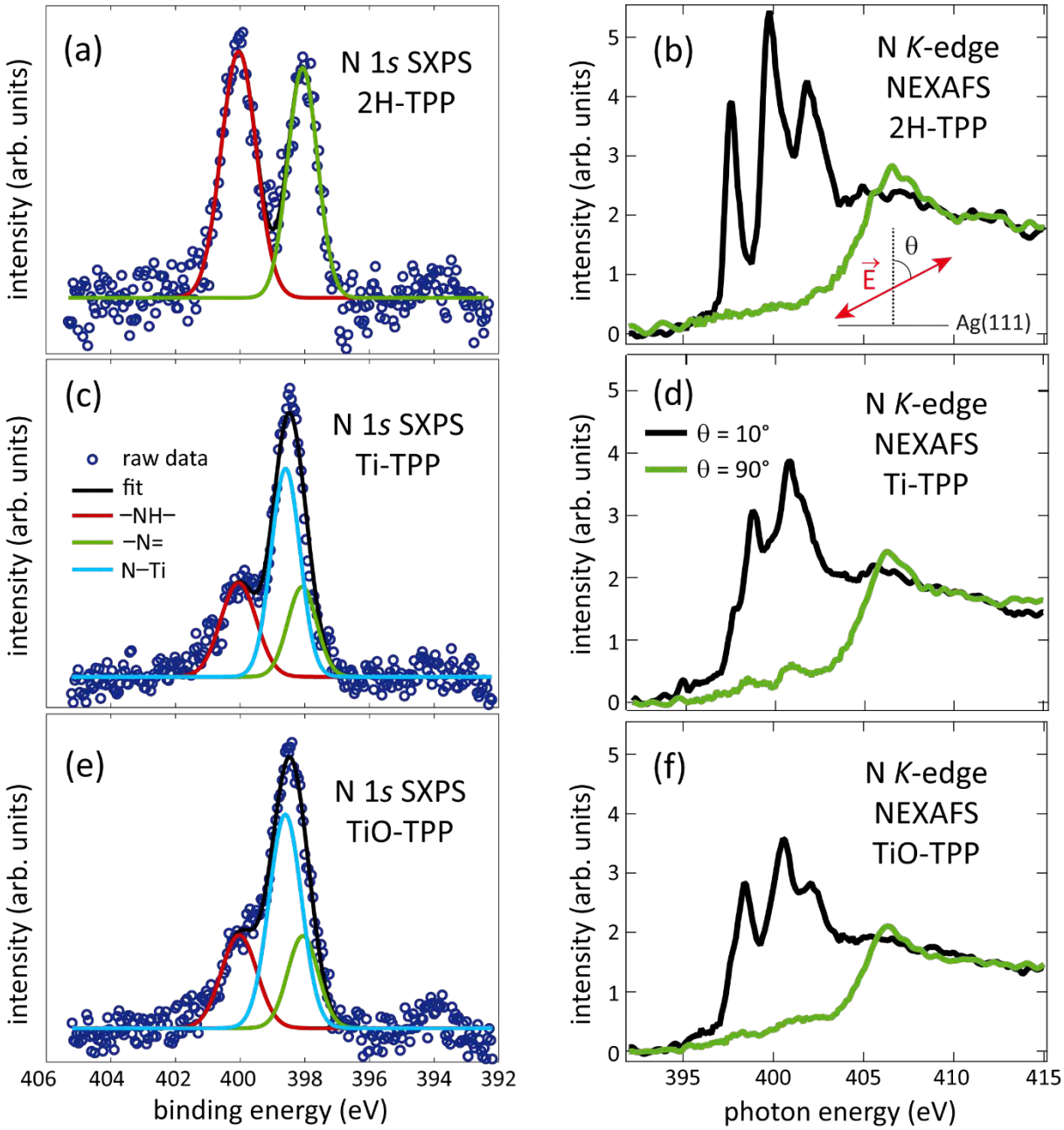

Figure 2: (a, c, e) Fitted N 1*s* SXPS with a photon energy of 550 eV (fitting parameters listed in Table S1 in SI) and (b, d, f) N *K*-edge NEXAFS measurements on the monolayer of (a, b) 2H-TPP, (c, d) Ti-TPP and (e, f) TiO-TPP (exposure: 200 L O_2) on Ag(111). The angle θ in the NEXAFS data defines the light polarization direction with respect to the surface normal. A comparable N *K*-edge NEXAFS spectrum for a fully metalated Ti-TPP layer, and its corresponding N 1*s* SXP spectrum, are shown in Figure S2 in the SI.

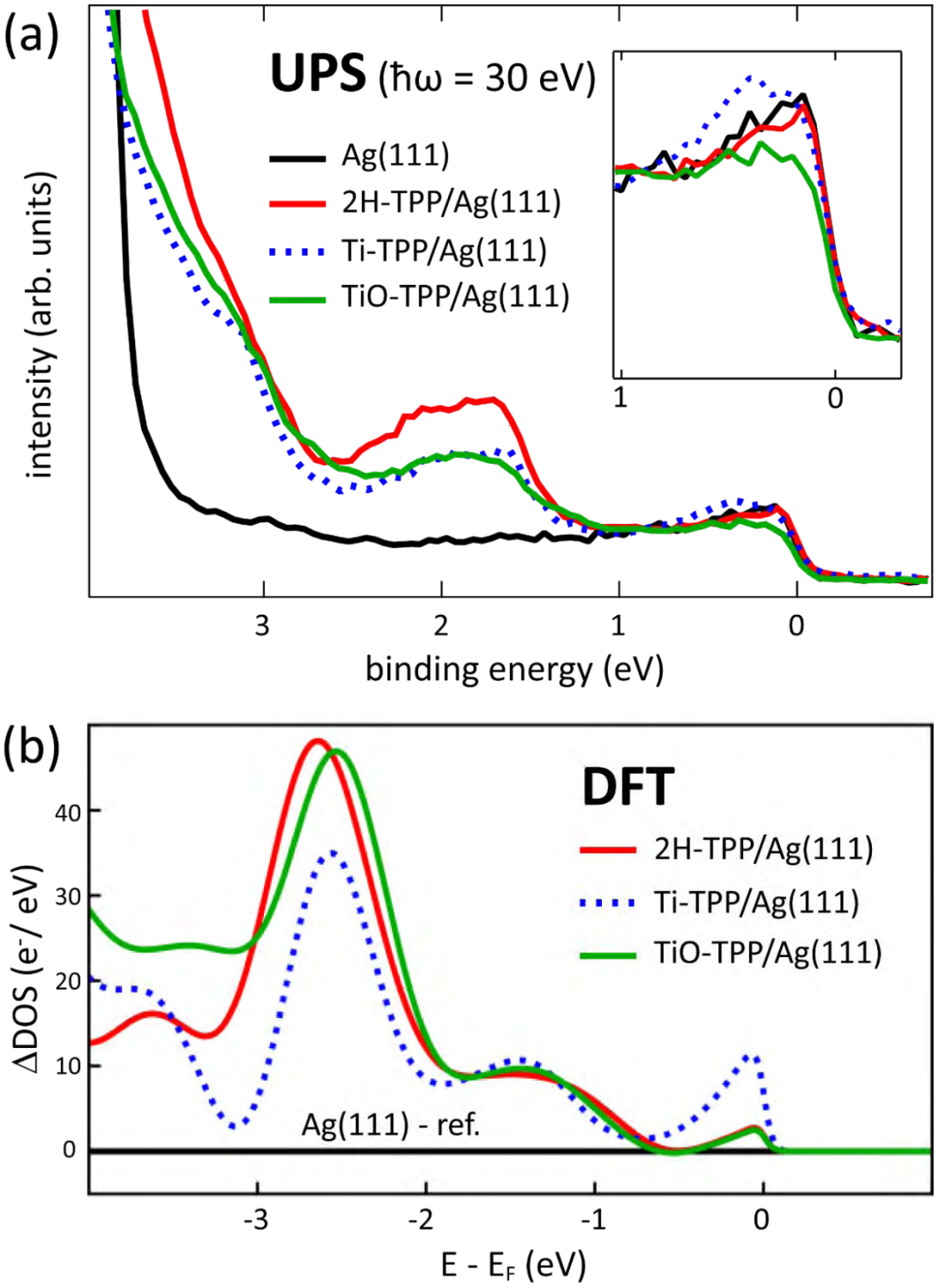

Figure 3: (a) UP spectra of 2H-TPP, Ti-TPP and TiO-TPP taken at photon energy of 30 eV along with the clean Ag(111) spectrum. The inset indicates the differences observed close to the Fermi edge, most notably the partial occupation of the Ti 3*d* related state (or, alternatively, of the former LUMO) after metalation with Ti, which is then lifted after exposure to molecular oxygen. (b) Calculated density of states (DOS) from DFT after subtraction of the DOS of the Ag(111) substrate. The energy scale is referred to the Fermi energy. Note that the fact that the calculated peak energies are about 0.5 – 1 eV closer to the Fermi edge than in the experiment is to be expected from a GGA-level description of the exchange-correlation term, also in combination with the vdW-density functionals.

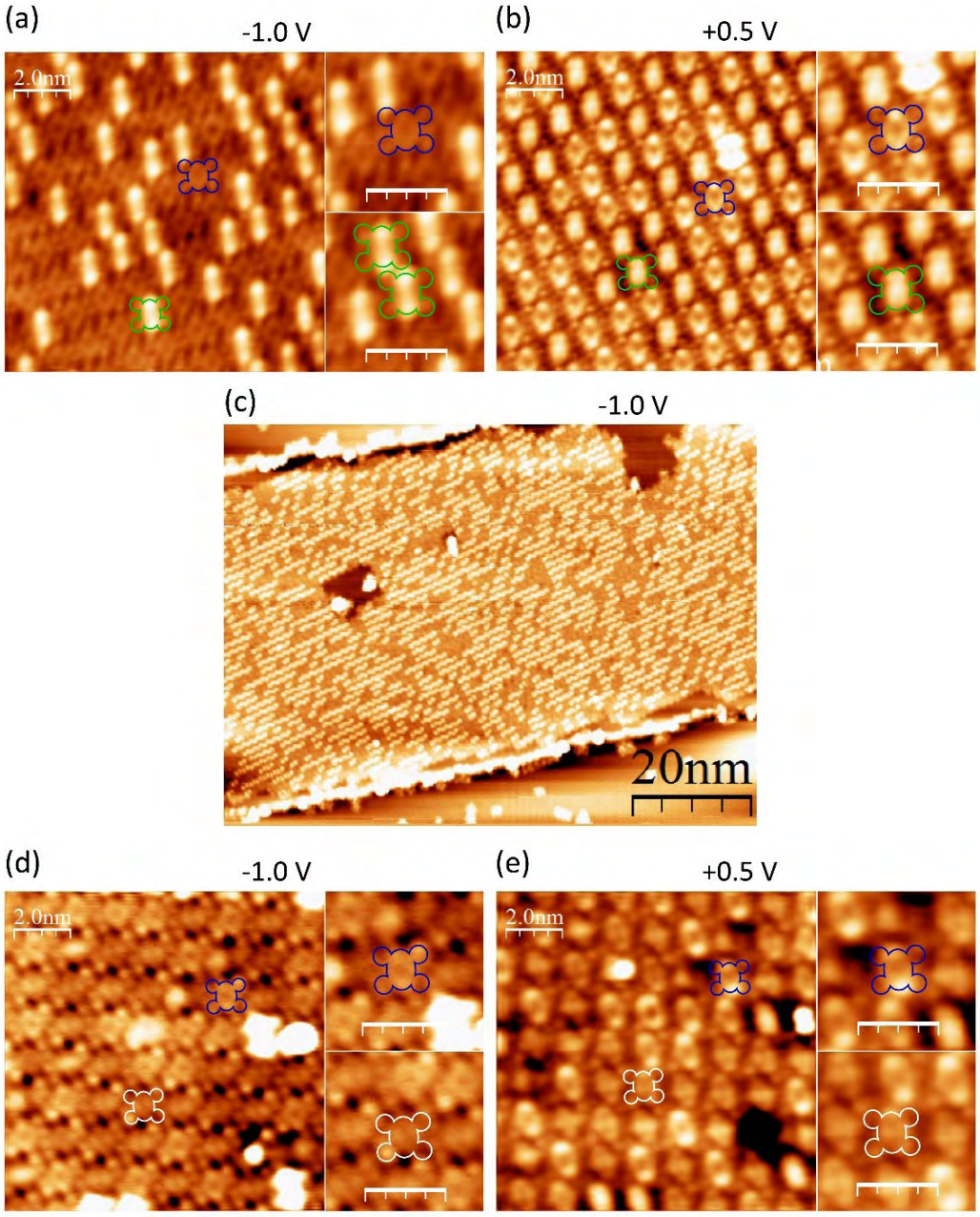

Figure 4: STM images of a (a, b, c) 2H-TPP island on Ag(111) after Ti deposition and annealing to 500 K, and (d, e) after exposure to 100 L of oxygen. The proposed appearance of the different species, (dark blue) 2H-TPP, (green) Ti-TPP and (white) TiO-TPP, is indicated by the overlaid shape. The zoomed in image of each species is shown next to the respective larger area image with the same (though rescaled) scale bar indicated in white. Note that the STM images in panels (a) and (b) are taken from the same area of the surface as the STM images in the supporting information of Ref.[9], but at a different bias (-0.1 V in our prior work). Tunneling current: (a, b) 0.2 nA, (c, d, e) 0.1 nA.

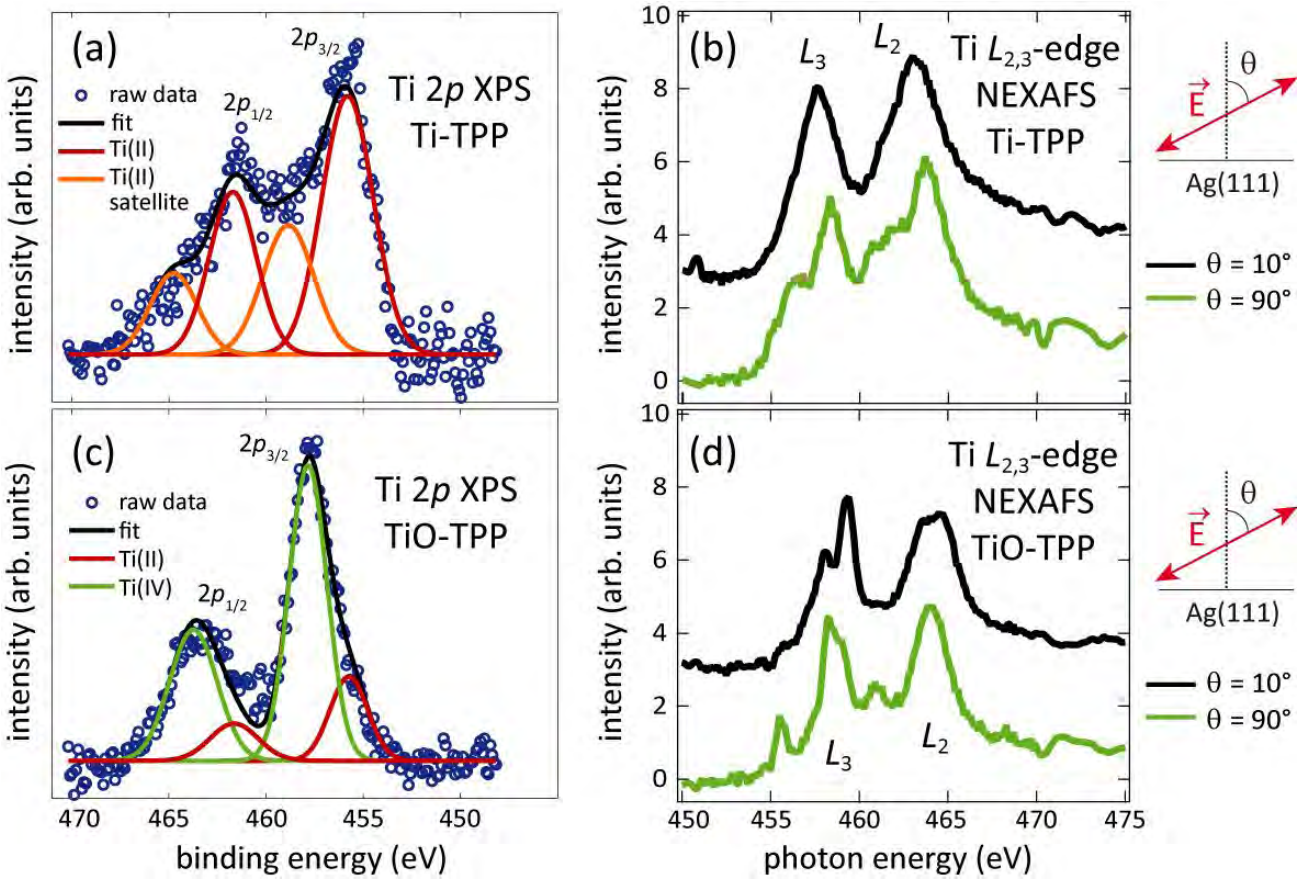

Figure 5: (a, c) Fitted Ti 2*p* XPS with Al *Kα* (fitting parameters listed in Table S1 in SI) and (b, d) Ti $L_{2,3}$-edge NEXAFS measurements of (a, b) Ti-TPP and (c, d) TiO-TPP on Ag(111). The individual NEXAFS spectra are vertically displaced for clarity. The Ti *2p* SXP spectra that correspond to the Ti $L_{2,3}$-edge NEXAFS in (b) and (d) are shown in Figure S3 in the SI. Panel (a) and (c) are adapted from Ref.[9] with permission from the Royal Society of Chemistry. Note that in panel (c) the O_2 exposure was 120 L, whereas in (d) the exposure was increased to 200 L to achieve a similar level of oxidation.

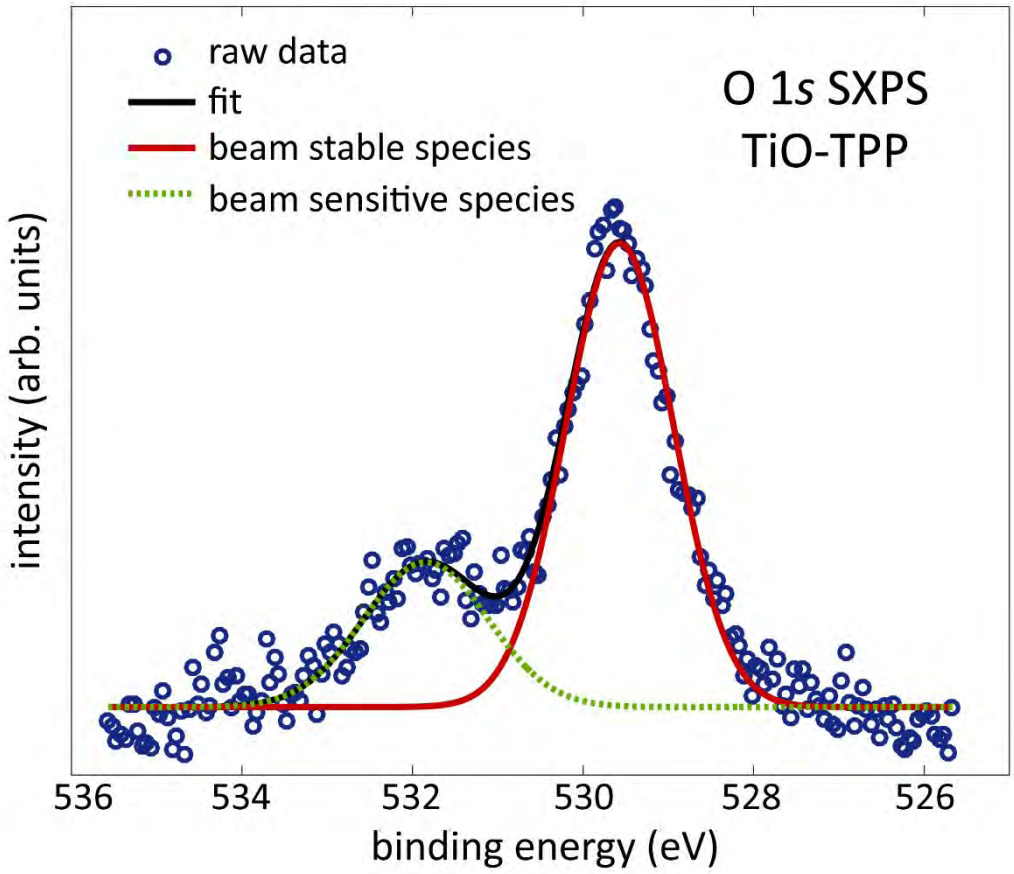

Figure 6: Fitted O 1*s* SXP spectrum of TiO-TPP on Ag(111) (exposure: 200 L O_2), recorded at a photon energy of 680 eV. The spectrum was fitted by two components: one component (red line) was found to be beam-stable and one (green dotted line) was found to be beam-sensitive. Fitting parameters are listed in Table S1 of the SI.

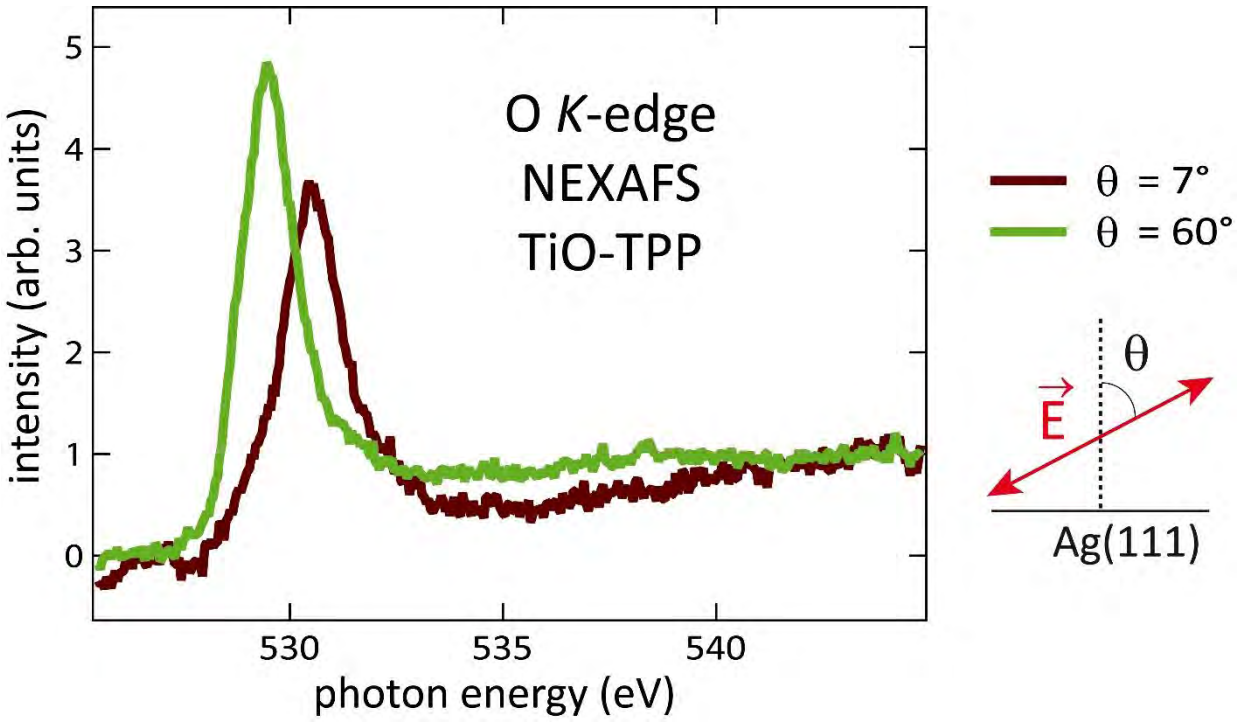

Figure 7: O *K*-edge NEXAFS from a monolayer of TiO-TPP on Ag(111) (exposure: 200 L O_2), measured with the photon polarization perpendicular to the surface (θ = 7°, out-of-plane polarization) and largely parallel to it (θ = 60°, in-plane polarization), respectively.

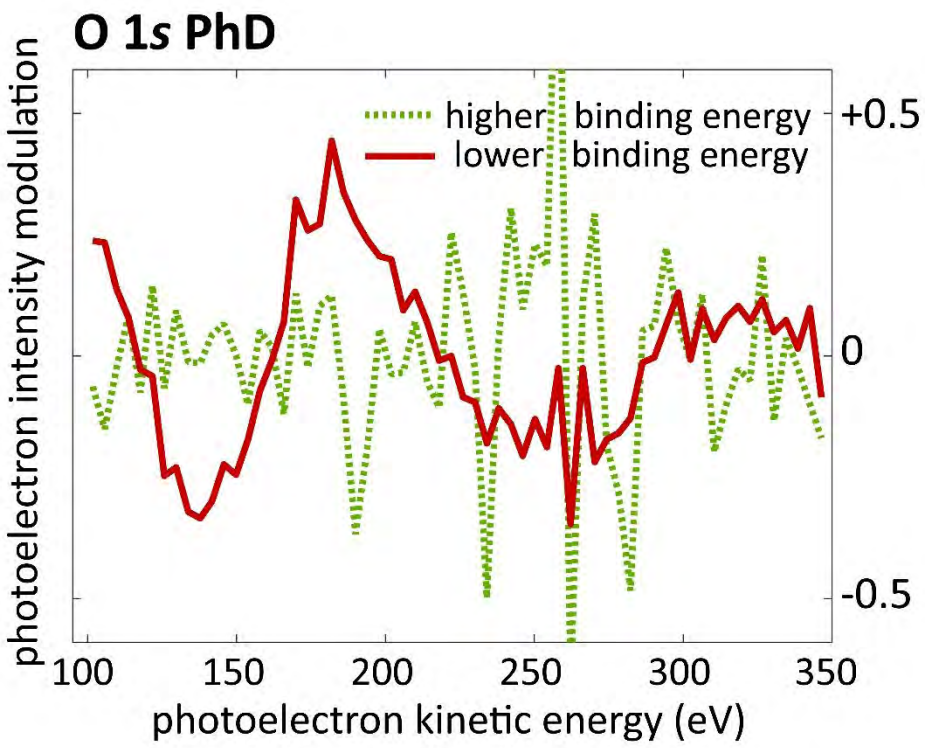

Figure 8: Comparison of the O 1*s* PhD modulations for the two different species observed in the O 1*s* SXP spectrum of Figure 6. The beam-stable feature with lower binding energy (red solid line; majority species) displays strong modulations as a function of the kinetic energy, whereas the beam-sensitive feature with higher binding energy (green dotted line) lacks these modulations completely.

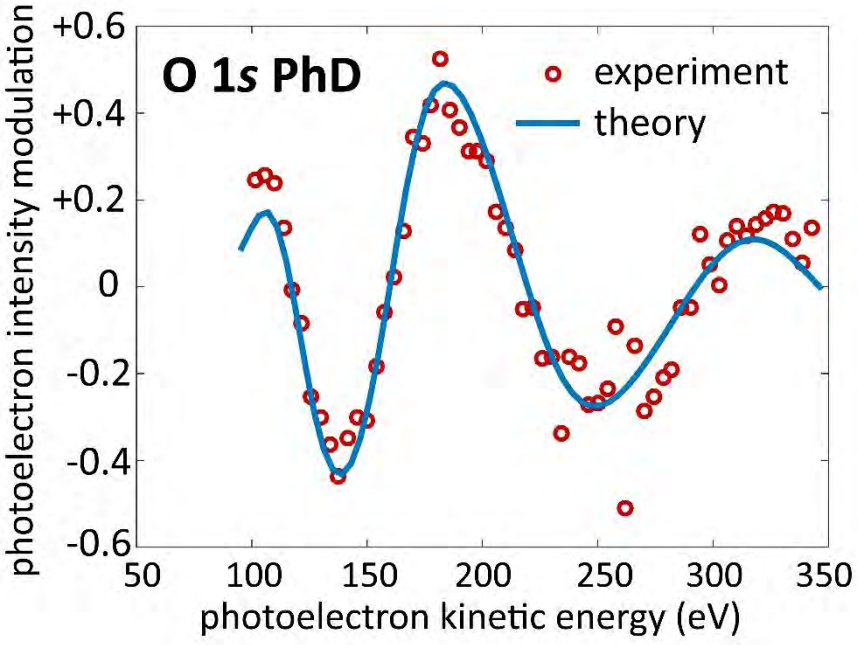

Figure 9: O 1*s* PhD: experiment-to-theory comparison for TiO-TPP on Ag(111) (majority species of Figures 6 and 8 only).

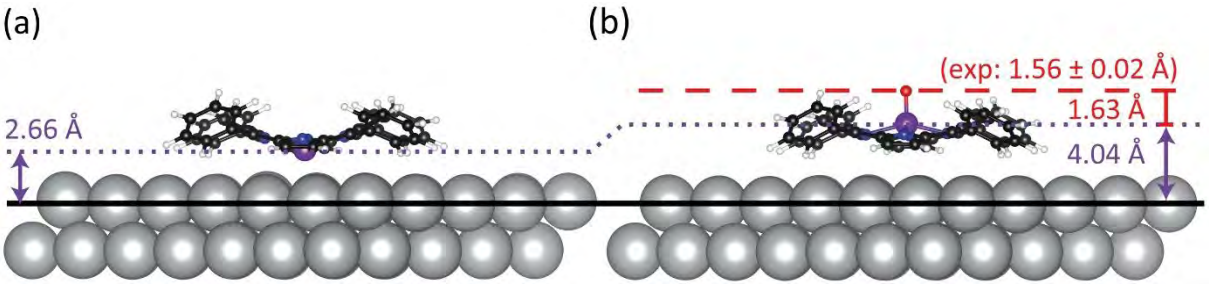

Figure 10: Schematic of the DFT-predicted adsorption structure of (a) Ti-TPP and (b) TiO-TPP on Ag(111). The adsorption height of the Ti atoms is shown in purple, and the Ti-O bond length in red with the experimentally measured value in brackets. White spheres are H atoms, black spheres C atoms, blue spheres N atoms, purple spheres Ti atoms, red spheres O atoms and large silver spheres Ag atoms.

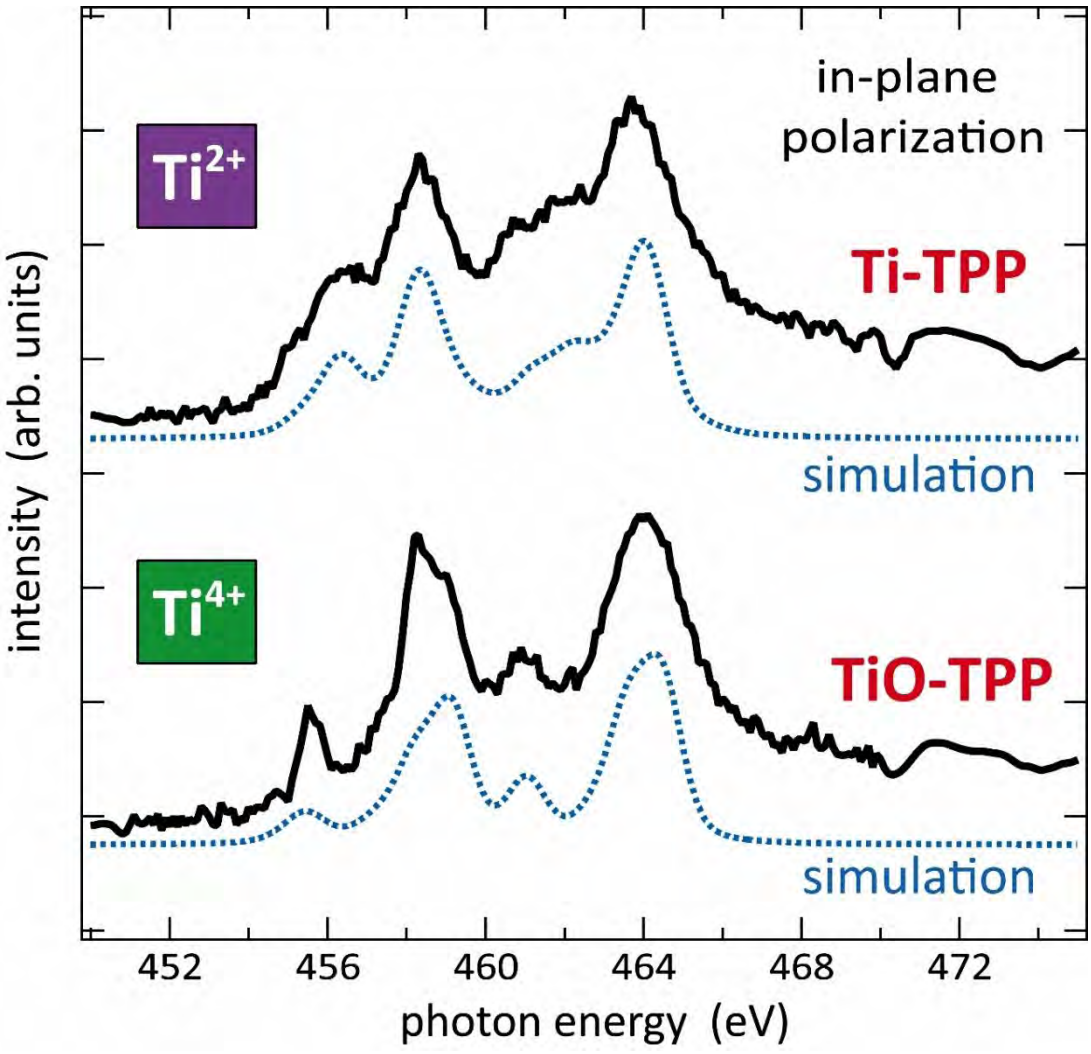

Figure 11: Comparison of experimental (black) and simulated (blue, dotted) Ti *L*-edge NEXAFS spectra. The simulated spectra were calculated using the CTM4XAS program, with polarization in the plane of the molecule(s); the experimental spectra were acquired with polarization parallel to the Ag(111) surface plane (and thus largely parallel to the macrocycle plane). The simulated spectra of Ti-TPP were shifted in energy by +2.2 eV to match the experimental data (see text).

References

1. Palomares, E.; Martinez-Diaz, M. V.; Haque, S. A.; Torres, T.; Durrant, J. R., State Selective Electron Injection in Non-Aggregated Titanium Phthalocyanine Sensitised Nanocrystalline TiO_2 Films. *Chem. Commun.* **2004**, 2112-2113.
2. Wäckerlin, C.; Chylarecka, D.; Kleibert, A.; Müller, K.; Iacovita, C.; Nolting, F.; Jung, T. A.; Ballav, N., Controlling Spins in Adsorbed Molecules by a Chemical Switch. *Nat. Commun.* **2010**, *1*, 61.
3. Ballav, N.; Wäckerlin, C.; Siewert, D.; Oppeneer, P. M.; Jung, T. A., Emergence of On-Surface Magnetochemistry. *J. Phys. Chem. Lett.* **2013**, *4*, 2303-2311.
4. Dougherty, D. B.; Sandin, A.; Vescovo, E.; Rowe, J. E., Coverage-Dependent Surface Magnetism of Iron Phthalocyanine on an O-Fe(110) Surface. *Phys. Rev. B* **2014**, *90*, 045406.
5. Xu, H.; Chen, R.; Sun, Q.; Lai, W.; Su, Q.; Huang, W.; Liu, X., Recent Progress in Metal-Organic Complexes for Optoelectronic Applications. *Chem. Soc. Rev.* **2014**, *43*, 3259-3302.
6. Copéret, C.; Chabanas, M.; Petroff Saint-Arroman, R.; Basset, J.-M., Homogeneous and Heterogeneous Catalysis: Bridging the Gap through Surface Organometallic Chemistry. *Angew. Chem. Int. Ed.* **2003**, *42*, 156-181.
7. Hulsken, B.; Van Hameren, R.; Gerritsen, J. W.; Khoury, T.; Thordarson, P.; Crossley, M. J.; Rowan, A. E.; Nolte, R. J. M.; Elemans, J. A. A. W.; Speller, S., Real-Time Single-Molecule Imaging of Oxidation Catalysis at a Liquid-Solid Interface. *Nat. Nano.* **2007**, *2*, 285-289.
8. Costentin, C.; Dridi, H.; Savéant, J.-M., Molecular Catalysis of O2 Reduction by Iron Porphyrins in Water: Heterogeneous Versus Homogeneous Pathways. *J. Am. Chem. Soc.* **2015**, *137*, 13535-13544.
9. Duncan, D. A.; Deimel, P. S.; Wiengarten, A.; Han, R.; Acres, R. G.; Auwärter, W.; Feulner, P.; Papageorgiou, A. C.; Allegretti, F.; Barth, J. V., Immobilised Molecular Catalysts and the Role of the Supporting Metal Substrate. *Chem. Commun.* **2015**, *51*, 9483-9486.
10. Mette, G.; Sutter, D.; Gurdal, Y.; Schnidrig, S.; Probst, B.; Iannuzzi, M.; Hutter, J.; Alberto, R.; Osterwalder, J., From Porphyrins to Pyrphyrins: Adsorption Study and Metalation of a Molecular Catalyst on Au(111). *Nanoscale* **2016**, *8*, 7958-7968.
11. Urbani, M.; Grätzel, M.; Nazeeruddin, M. K.; Torres, T., Meso-Substituted Porphyrins for Dye-Sensitized Solar Cells. *Chem. Rev.* **2014**, *114*, 12330-12396.
12. Mathew, S.; Yella, A.; Gao, P.; Humphry-Baker, R.; CurchodBasile, F. E.; Ashari-Astani, N.; Tavernelli, I.; Rothlisberger, U.; NazeeruddinMd, K.; Grätzel, M., Dye-Sensitized Solar Cells with 13% Efficiency Achieved through the Molecular Engineering of Porphyrin Sensitizers. *Nat. Chem.* **2014**, *6*, 242-247.
13. Arrowsmith, R. L.; Pascu, S. I.; Smugowski, H., New Developments in the Biomedical Chemistry of Metal Complexes: From Small Molecules to Nanotheranostic Design. *Organomet. Chem.* **2012**, *38*, 1-35.
14. Ma, D.-L.; He, H.-Z.; Leung, K.-H.; Chan, D. S.-H.; Leung, C.-H., Bioactive Luminescent Transition-Metal Complexes for Biomedical Applications. *Angew. Chem. Int. Ed.* **2013**, *52*, 7666-7682.
15. Gottfried, J. M., Surface Chemistry of Porphyrins and Phthalocyanines. *Surf. Sci. Rep.* **2015**, *70*, 259-379.
16. Auwärter, W.; Écija, D.; Klappenberger, F.; Barth, J. V., Porphyrins at Interfaces. *Nat. Chem.* **2015**, *7*, 105-120.
17. Boaz, N. C.; Bell, S. R.; Groves, J. T., Ferryl Protonation in Oxoiron(Iv) Porphyrins and Its Role in Oxygen Transfer. *J. Am. Chem. Soc.* **2015**, *137*, 2875-2885.
18. Shing, K.-P.; Cao, B.; Liu, Y.; Lee, H. K.; Li, M.-D.; Phillips, D. L.; Chang, X.-Y.; Che, C.-M., Arylruthenium(Iii) Porphyrin-Catalyzed C–H Oxidation and Epoxidation at Room Temperature and [Ruv(Por)(O)(Ph)] Intermediate by Spectroscopic Analysis and Density Functional Theory Calculations. *J. Am. Chem. Soc.* **2018**, *140*, 7032-7042.
19. Song, W. J.; Seo, M. S.; DeBeer George, S.; Ohta, T.; Song, R.; Kang, M.-J.; Tosha, T.; Kitagawa, T.; Solomon, E. I.; Nam, W., Synthesis, Characterization, and Reactivities of Manganese(V)−Oxo Porphyrin Complexes. *J. Am. Chem. Soc.* **2007**, *129*, 1268-1277.
20. Jin, N.; Ibrahim, M.; Spiro, T. G.; Groves, J. T., Trans-Dioxo Manganese(V) Porphyrins. *J. Am. Chem. Soc.* **2007**, *129*, 12416-12417.

21. Murphy, B. E.; Krasnikov, S. A.; Sergeeva, N. N.; Cafolla, A. A.; Preobrajenski, A. B.; Chaika, A. N.; Lübben, O.; Shvets, I. V., Homolytic Cleavage of Molecular Oxygen by Manganese Porphyrins Supported on Ag(111). *ACS Nano* **2014**, *8*, 5190-5198.
22. Sobolewski, A. L.; Domcke, W., Photoinduced Water Splitting with Oxotitanium Porphyrin: A Computational Study. *Phys. Chem. Chem. Phys.* **2012**, *14*, 12807-12817.
23. Morawski, O.; Izdebska, K.; Karpiuk, E.; Nowacki, J.; Suchocki, A.; Sobolewski, A. L., Photoinduced Water Splitting with Oxotitanium Tetraphenylporphyrin. *Phys. Chem. Chem. Phys.* **2014**, *16*, 15256-15262.
24. Pantel, R.; Levy, D.; Nicolas, D., Auger Electron Spectroscopy Technique for Nitrogen Depth Profiling in Titanium Compounds. *J. Vac. Sci, Technol. A* **1988**, *6*, 2953-2956.
25. Guillot, J.; Wirtz, T.; Girot, T.; Penoy, M.; Migeon, H. N.; Barbier, G., Quantification of a Ti(C_xn_{1-x}) Based Multilayer by Auger Electron Spectroscopy. *Appl. Surf. Sci.* **2009**, *256*, 773-778.
26. Naumkin, A. V.; Kraut-Vass, A.; Gaarenstroom, S. W.; Powell, C. J., *NIST X-Ray Photoelectron Spectroscopy Database*, Version 4.1; National Institute of Standards and Technology: Gaithersburg, 2012. https://srdata.nist.gov/xps/.
27. Seah, M. P.; Smith, G. C.; Anthony, M. T., Aes: Energy Calibration of Electron Spectrometers. I—an Absolute, Traceable Energy Calibration and the Provision of Atomic Reference Line Energies. *Surf. Interface Anal.* **1990**, *15*, 293-308.
28. Woodruff, D. P.; Bradshaw, A. M., Adsorbate Structure Determination on Surfaces Using Photoelectron Diffraction. *Rep. Progr. Phys.* **1994**, *57*, 1029-1029.
29. Woodruff, D. P., Absorbate Structure Deterermination Using Photoelectron Diffraction: Methods and Applications. *Surf. Sci. Rep.* **2007**, *62*, 1-38.
30. Fritzsche, V., Approximations for Photoelectron Scattering. *Surf. Sci.* **1989**, *213*, 648-656.
31. Fritzsche, V., A New Spherical-Wave Approximation for Photoelectron Diffraction, EXAFS and MEED. *J. Phys.: Condens. Matter* **1990**, *2*, 1413-1413.
32. Fritzsche, V., Calculation of Auger Electron Diffraction at a Ni(111) Surface. *J. Phys.: Condens. Matter* **1990**, *2*, 9735-9735.
33. Fritzsche, V., Consequences of a Finite-Energy Resolution for Photoelectron Diffraction Spectra. *Surf. Sci.* **1992**, *265*, 187-195.
34. Fritzsche, V.; Pendry, J. B., Linear-Superposition Method for the Multiple-Scattering Problem in Low-Energy-Photoelectron Diffraction. *Phys. Rev. B* **1993**, *48*, 9054---9054.
35. Fritzsche, V.; Davis, R.; Hu, X. M.; Woodruff, D. P.; Weiss, K. U.; Dippel, R.; Schindler, K. M.; Hofmann, P.; Bradshaw, A. M., Initial State Effects in Scanned Energy Mode Photoelectron Diffraction. *Phys Rev B* **1994**, *49*, 7729-7729.
36. Duncan, D. A.; Choi, J. I. J.; Woodruff, D. P., Global Search Algorithms in Surface Structure Determination Using Photoelectron Diffraction. *Surf. Sci.* **2012**, *606*, 278-284.
37. Horcas, I.; Fernández, R.; Gómez-Rodríguez, J. M.; Colchero, J.; Gómez-Herrero, J.; Baro, A. M., Wsxm: A Software for Scanning Probe Microscopy and a Tool for Nanotechnology. *Rev. Sci. Instrum.* **2007**, *78*, 013705.
38. Stavitski, E.; de Groot, F. M. F., The Ctm4xas Program for Eels and Xas Spectral Shape Analysis of Transition Metal L Edges. *Micron* **2010**, *41*, 687-694.
39. Johnson, P. S.; García-Lastra, J. M.; Kennedy, C. K.; Jersett, N. J.; Boukahil, I.; Himpsel, F. J.; Cook, P. L., Crystal Fields of Porphyrins and Phthalocyanines from Polarization-Dependent 2p-to-3d Multiplets. *J. Chem. Phys.* **2014**, *140*, 114706.
40. Pickup, D. F.; Zegkinoglou, I.; Ballesteros, B.; Ganivet, C. R.; García-Lastra, J. M.; Cook, P. L.; Johnson, P. S.; Rogero, C.; de Groot, F.; Rubio, A., et al., Influence of Axial and Peripheral Ligands on the Electronic Structure of Titanium Phthalocyanines. *J. Phys. Chem. C* **2013**, *117*, 4410-4420.
41. Giannozzi, P.; Baroni, S.; Bonini, N.; Calandra, M.; Car, R.; Cavazzoni, C.; Ceresoli, D.; Chiarotti, G. L.; Cococcioni, M.; Dabo, I., et al., Quantum Espresso: A Modular and Open-Source Software Project for Quantum Simulations of Materials. *J. Phys.: Condens. Matter* **2009**, *21*, 395502, www.Quantum-ESPRESSO.org/.
42. Hamada, I., Van Der Waals Density Functional Made Accurate. *Phys. Rev. B* **2014**, *89*, 121103.

43. Blöchl, P. E., Projector Augmented-Wave Method. *Phys. Rev. B* **1994**, *50*, 17953-17979.
44. Auwärter, W.; Seufert, K.; Klappenberger, F.; Reichert, J.; Weber-Bargioni, A.; Verdini, A.; Cvetko, D.; Dell'Angela, M.; Floreano, L.; Cossaro, A., et al., Site-Specific Electronic and Geometric Interface Structure of Co-Tetraphenyl-Porphyrin Layers on Ag(111). *Phys. Rev. B* **2010**, *81*, 245403.
45. Zaglmayr, H.; Lackner, T.; Sun, L.; Zeppenfeld, P., Growth of Tetraphenyl-Porphyrin Thin Films on Ag(111). *Synth. Met.* **2017**, *228*, 64-69.
46. Buchner, F.; Flechtner, K.; Bai, Y.; Zillner, E.; Kellner, I.; Steinrück, H.-P.; Marbach, H.; Gottfried, J. M., Coordination of Iron Atoms by Tetraphenylporphyrin Monolayers and Multilayers on Ag(111) and Formation of Iron-Tetraphenylporphyrin. *J. Phys. Chem. C* **2008**, *112*, 15458-15465.
47. Papageorgiou, A. C.; Fischer, S.; Oh, S. C.; Sağlam, Ö.; Reichert, J.; Wiengarten, A.; Seufert, K.; Vijayaraghavan, S.; Écija, D.; Auwärter, W., et al., Self-Terminating Protocol for an Interfacial Complexation Reaction in Vacuo by Metal–Organic Chemical Vapor Deposition. *ACS Nano* **2013**, *7*, 4520-4526.
48. Marbach, H., Surface-Mediated in Situ Metalation of Porphyrins at the Solid–Vacuum Interface. *Acc. Chem. Res.* **2015**, *48*, 2649-2658.
49. Diller, K.; Papageorgiou, A. C.; Klappenberger, F.; Allegretti, F.; Barth, J. V.; Auwärter, W., In Vacuo Interfacial Tetrapyrrole Metallation. *Chem. Soc. Rev.* **2016**, *45*, 1629-1656.
50. Gottfried, J. M.; Flechtner, K.; Kretschmann, A.; Lukasczyk, T.; Steinrück, H.-P., Direct Synthesis of a Metalloporphyrin Complex on a Surface. *J. Am. Chem. Soc.* **2006**, *128*, 5644-5645.
51. Di Santo, G.; Castellarin-Cudia, C.; Fanetti, M.; Taleatu, B.; Borghetti, P.; Sangaletti, L.; Floreano, L.; Magnano, E.; Bondino, F.; Goldoni, A., Conformational Adaptation and Electronic Structure of 2H-Tetraphenylporphyrin on Ag(111) During Fe Metalation. *J. Phys. Chem. C* **2011**, *115*, 4155-4162.
52. Di Santo, G.; Blankenburg, S.; Castellarin-Cudia, C.; Fanetti, M.; Borghetti, P.; Sangaletti, L.; Floreano, L.; Verdini, A.; Magnano, E.; Bondino, F., et al., Supramolecular Engineering through Temperature-Induced Chemical Modification of 2H-Tetraphenylporphyrin on Ag(111): Flat Phenyl Conformation and Possible Dehydrogenation Reactions. *Chem. Eur. J.* **2011**, *17*, 14354-14359.
53. Diller, K.; Klappenberger, F.; Marschall, M.; Hermann, K.; Nefedov, A.; Wöll, C.; Barth, J. V., Self-Metalation of 2h-Tetraphenylporphyrin on Cu(111): An X-Ray Spectroscopy Study. *J. Chem. Phys.* **2012**, *136*, 014705.
54. Rojas, G.; Chen, X.; Bravo, C.; Kim, J.-H.; Kim, J.-S.; Xiao, J.; Dowben, P. A.; Gao, Y.; Zeng, X. C.; Choe, W., et al., Self-Assembly and Properties of Nonmetalated Tetraphenyl-Porphyrin on Metal Substrates. *J. Phys. Chem. C* **2010**, *114*, 9408-9415.
55. Buchner, F.; Kellner, I.; Hieringer, W.; Gorling, A.; Steinruck, H.-P.; Marbach, H., Ordering Aspects and Intramolecular Conformation of Tetraphenylporphyrins on Ag(111). *Phys. Chem. Chem. Phys.* **2010**, *12*, 13082-13090.
56. Jennings, W. B.; Farrell, B. M.; Malone, J. F., Attractive Intramolecular Edge-to-Face Aromatic Interactions in Flexible Organic Molecules. *Acc. Chem. Res.* **2001**, *34*, 885-894.
57. Buchner, F.; Zillner, E.; Röckert, M.; Gläßel, S.; Steinrück, H.-P.; Marbach, H., Substrate-Mediated Phase Separation of Two Porphyrin Derivatives on Cu(111). *Chem. Eur. J.* **2011**, *17*, 10226-10229.
58. Auwärter, W.; Weber-Bargioni, A.; Brink, S.; Riemann, A.; Schiffrin, A.; Ruben, M.; Barth, J. V., Controlled Metalation of Self-Assembled Porphyrin Nanoarrays in Two Dimensions. *ChemPhysChem* **2007**, *8*, 250-254.
59. Auwärter, W.; Seufert, K.; Bischoff, F.; Écija, D.; Vijayaraghavan, S.; Joshi, S.; Klappenberger, F.; Samudrala, N.; Barth, J. V., A Surface-Anchored Molecular Four-Level Conductance Switch Based on Single Proton Transfer. *Nat. Nano.* **2012**, *7*, 41-46.
60. Röckert, M.; Franke, M.; Tariq, Q.; Lungerich, D.; Jux, N.; Stark, M.; Kaftan, A.; Ditze, S.; Marbach, H.; Laurin, M., et al., Insights in Reaction Mechanistics: Isotopic Exchange During the Metalation of Deuterated Tetraphenyl-21,23d-Porphyrin on Cu(111). *J. Phys. Chem. C* **2014**, *118*, 26729-26736.

61. Weber-Bargioni, A.; Auwärter, W.; Klappenberger, F.; Reichert, J.; Lefrançois, S.; Strunskus, T.; Wöll, C.; Schiffrin, A.; Pennec, Y.; Barth, J. V., Visualizing the Frontier Orbitals of a Conformationally Adapted Metalloporphyrin. *ChemPhysChem* **2008**, *9*, 89-94.
62. Sedona, F.; Rizzi, G. A.; Agnoli, S.; Llabrés i Xamena, F. X.; Papageorgiou, A.; Ostermann, D.; Sambi, M.; Finetti, P.; Schierbaum, K.; Granozzi, G., Ultrathin Tio_x Films on Pt(111): A LEED, XPS, and STM Investigation. *J. Phys. Chem. B* **2005**, *109*, 24411-24426.
63. Oku, M.; Wagatsuma, K.; Kohiki, S., Ti 2p and Ti 3p X-Ray Photoelectron Spectra for TiO_2, $SrTiO_3$ and $BaTiO_3$. *Phys. Chem. Chem. Phys.* **1999**, *1*, 5327-5331.
64. Groot, F. d., Multiplet Effects in X-Ray Spectroscopy. *Coord. Chem. Rev.* **2005**, *249*, 31-63.
65. Biesinger, M. C.; Lau, L. W. M.; Gerson, A. R.; Smart, R. S. C., Resolving Surface Chemical States in XPS Analysis of First Row Transition Metals, Oxides and Hydroxides: Sc, Ti, V, Cu and Zn. *Appl. Surf. Sci.* **2010**, *257*, 887-898.
66. Grosvenor, A. P.; Kobe, B. A.; Biesinger, M. C.; McIntyre, N. S., Investigation of Multiplet Splitting of Fe 2p XPS Spectra and Bonding in Iron Compounds. *Surf. Interface Anal.* **2004**, *36*, 1564-1574.
67. Gupta, R. P.; Sen, S. K., Calculation of Multiplet Structure of Core *p*-Vacancy Levels, II. *Phys. Rev. B* **1975**, *12*, 15-19.
68. Jaeger, D.; Patscheider, J., A Complete and Self-Consistent Evaluation of XPS Spectra of Tin. *J. Electron Spectrosc. Relat. Phenom.* **2012**, *185*, 523-534.
69. Jaeger, D.; Patscheider, J., Single Crystalline Oxygen-Free Titanium Nitride by XPS. *Surf. Sci. Spectra* **2013**, *20*, 1-8.
70. Henderson, G. S.; Liu, X.; Fleet, M. E., A Ti L-Edge X-Ray Absorption Study of Ti-Silicate Glasses. *Phys. Chem. Miner.* **2002**, *29*, 32-42.
71. Stoyanov, E.; Langenhorst, F.; Steinle-Neumann, G., The Effect of Valence State and Site Geometry on Ti $L_{3,2}$ and O K Electron Energy-Loss Spectra of Ti_xO_y Phases. *Am. Mineral.* **2007**, *92*, 577-586.
72. Zhou, J. G.; Fang, H. T.; Maley, J. M.; Murphy, M. W.; Peter Ko, J. Y.; Cutler, J. N.; Sammynaiken, R.; Sham, T. K.; Liu, M.; Li, F., Electronic Structure of TiO_2 Nanotube Arrays from X-Ray Absorption near Edge Structure Studies. *J. Mater. Chem.* **2009**, *19*, 6804-6809.
73. de Groot, F. M. F.; Fuggle, J. C.; Thole, B. T.; Sawatzky, G. A., $L_{2,3}$ X-Ray-Absorption Edges of d^0 Compounds: K^+, Ca^{2+}, Sc^{3+}, and Ti^{4+} in O_h (Octahedral) Symmetry. *Phys. Rev. B* **1990**, *41*, 928-937.
74. Caretti, I.; Yuste, M.; Torres, R.; Sanchez, O.; Jimenez, I.; Escobar Galindo, R., Coordination Chemistry of Titanium and Zinc in $Ti_{(1-x)}Zn_{2x}O_2$ ($0 < X < 1$) Ultrathin Films Grown by DC Reactive Magnetron Sputtering. *RSC Adv.* **2012**, *2*, 2696-2699.
75. Tian, H.; Schryvers, D.; Liu, D.; Jiang, Q.; Van Humbeeck, J., Stability of Ni in Nitinol Oxide Surfaces. *Acta Biomater.* **2011**, *7*, 892-899.
76. Lukasczyk, T.; Flechtner, K.; Merte, L. R.; Jux, N.; Maier, F.; Gottfried, J. M.; Steinrück, H.-P., Interaction of Cobalt(II) Tetraarylporphyrins with a Ag(111) Surface Studied with Photoelectron Spectroscopy. *J. Phys. Chem. C* **2007**, *111*, 3090-3098.
77. Seufert, K.; Bocquet, M.-L.; Auwärter, W.; Weber-Bargioni, A.; Reichert, J.; Lorente, N.; Barth, J. V., Cis-Dicarbonyl Binding at Cobalt and Iron Porphyrins with Saddle-Shape Conformation. *Nat. Chem.* **2011**, *3*, 114.
78. Häming, M.; Scheuermann, C.; Schöll, A.; Reinert, F.; Umbach, E., Coverage Dependent Organic–Metal Interaction Studied by High-Resolution Core Level Spectroscopy: Snpc (Sub)Monolayers on Ag(111). *J. Electron Spectrosc. Relat. Phenom.* **2009**, *174*, 59-64.
79. Bischoff, F.; Seufert, K.; Auwärter, W.; Joshi, S.; Vijayaraghavan, S.; Écija, D.; Diller, K.; Papageorgiou, A. C.; Fischer, S.; Allegretti, F., et al., How Surface Bonding and Repulsive Interactions Cause Phase Transformations: Ordering of a Prototype Macrocyclic Compound on Ag(111). *ACS Nano* **2013**, *7*, 3139-3149.
80. Lerch, A.; Fernandez, L.; Ilyn, M.; Gastaldo, M.; Paradinas, M.; Valbuena, M. A.; Mugarza, A.; Ibrahim, A. B. M.; Sundermeyer, J.; Höfer, U., et al., Electronic Structure of Titanylphthalocyanine Layers on Ag(111). *J. Phys. Chem. C* **2017**, *121*, 25353-25363.

81. Duncan, D. A.; Unterberger, W.; Hogan, K. A.; Lerotholi, T. J.; Lamont, C. L. A.; Woodruff, D. P., A Photoelectron Diffraction Investigation of Vanadyl Phthalocyanine on Au(111). *Surf. Sci.* **2010**, *604*, 47-53.
82. Kröger, I.; Stadtmüller, B.; Kumpf, C., Submonolayer and Multilayer Growth of Titaniumoxide-Phthalocyanine on Ag(111). *New J. Phys.* **2016**, *18*, 113022.
83. Deimel, P. S.; Bababrik, R. M.; Wang, B.; Blowey, P. J.; Rochford, L. A.; Thakur, P. K.; Lee, T.-L.; Bocquet, M.-L.; Barth, J. V.; Woodruff, D. P., et al., Direct Quantitative Identification of the "Surface Trans-Effect". *Chem.Sci.* **2016**, *7*, 5647-5656.
84. Guilard, R.; Latour, J. M.; Lecomte, C.; Marchon, J. C.; Protas, J.; Ripoll, D., Peroxotitanium(IV) Porphyrins. Synthesis, Stereochemistry, and Properties. *Inorg. Chem.* **1978**, *17*, 1228-1237.
85. Zakharov, A. V.; Shlykov, S. A.; Zhabanov, Y. A.; Girichev, G. V., The Structure of Oxotitanium Phthalocyanine: A Gas-Phase Electron Diffraction and Computational Study. *Phys. Chem. Chem. Phys.* **2009**, *11*, 3472-3477.
86. Diller, K.; Klappenberger, F.; Allegretti, F.; Papageorgiou, A. C.; Fischer, S.; Wiengarten, A.; Joshi, S.; Seufert, K.; Écija, D.; Auwärter, W., et al., Investigating the Molecule-Substrate Interaction of Prototypic Tetrapyrrole Compounds: Adsorption and Self-Metalation of Porphine on Cu(111). *J. Chem. Phys.* **2013**, *138*, 154710.
87. Müller, M.; Diller, K.; Maurer, R. J.; Reuter, K., Interfacial Charge Rearrangement and Intermolecular Interactions: Density-Functional Theory Study of Free-Base Porphine Adsorbed on Ag(111) and Cu(111). *J. Chem. Phys.* **2016**, *144*, 024701.
88. Du, G.; Mirafzal, G. A.; Woo, L. K., Reductive Coupling Reactions of Carbonyl Compounds with a Low-Valent Titanium(II) Porphyrin Complex. *Organometallics* **2004**, *23*, 4230-4235.
89. Wijeratne, G. B.; Zolnhofer, E. M.; Fortier, S.; Grant, L. N.; Carroll, P. J.; Chen, C.-H.; Meyer, K.; Krzystek, J.; Ozarowski, A.; Jackson, T. A., et al., Electronic Structure and Reactivity of a Well-Defined Mononuclear Complex of Ti(II). *Inorg. Chem.* **2015**, *54*, 10380-10397.
90. Gauvin, R. M.; Buch, F.; Delevoye, L.; Harder, S., Well-Defined Silica-Supported Calcium Reagents: Control of Schlenk Equilibrium by Grafting. *Chem. Eur. J.* **2009**, *15*, 4382-4393.
91. Wäckerlin, C.; Tarafder, K.; Siewert, D.; Girovsky, J.; Hahlen, T.; Iacovita, C.; Kleibert, A.; Nolting, F.; Jung, T. A.; Oppeneer, P. M., et al., On-Surface Coordination Chemistry of Planar Molecular Spin Systems: Novel Magnetochemical Effects Induced by Axial Ligands. *Chem.Sci.* **2012**, *3*, 3154-3160.
92. Hieringer, W.; Flechtner, K.; Kretschmann, A.; Seufert, K.; Auwärter, W.; Barth, J. V.; Görling, A.; Steinrück, H.-P.; Gottfried, J. M., The Surface Trans Effect: Influence of Axial Ligands on the Surface Chemical Bonds of Adsorbed Metalloporphyrins. *J. Am. Chem. Soc.* **2011**, *133*, 6206-6222.
93. Flechtner, K.; Kretschmann, A.; Steinrück, H.-P.; Gottfried, J. M., No-Induced Reversible Switching of the Electronic Interaction between a Porphyrin-Coordinated Cobalt Ion and a Silver Surface. *J. Am. Chem. Soc.* **2007**, *129*, 12110-12111.
94. Chen, W.; Wang, L.; Qi, D. C.; Chen, S.; Gao, X. Y.; Wee, A. T. S., Probing the Ultrafast Electron Transfer at the Cupc/Au(111) Interface. *Appl. Phys. Lett.* **2006**, *88*, 184102.
95. Köbl, J.; Wang, T.; Wang, C.; Drost, M.; Tu, F.; Xu, Q.; Ju, H.; Wechsler, D.; Franke, M.; Pan, H., et al., Hungry Porphyrins: Protonation and Self-Metalation of Tetraphenylporphyrin on TiO_2(110) - 1 × 1. *ChemistrySelect* **2016**, *1*, 6103-6105.
96. Lovat, G.; Forrer, D.; Abadia, M.; Dominguez, M.; Casarin, M.; Rogero, C.; Vittadini, A.; Floreano, L., Very High Temperature Tiling of Tetraphenylporphyrin on Rutile TiO_2(110). *Nanoscale* **2017**, *9*, 11694-11704.
97. Wechsler, D.; Fernández, C. C.; Steinrück, H.-P.; Lytken, O.; Williams, F. J., Covalent Anchoring and Interfacial Reactions of Adsorbed Porphyrins on Rutile TiO_2(110). *J. Phys. Chem. C* **2018**, *122*, 4480-4487.
98. Kollhoff, F.; Schneider, J.; Li, G.; Barkaoui, S.; Shen, W.; Berger, T.; Diwald, O.; Libuda, J., Anchoring of Carboxyl-Functionalized Porphyrins on MgO, TiO_2, and Co_3O_4 Nanoparticles. *Phys. Chem. Chem. Phys.* **2018**, *20*, 24858-24868.

(a)

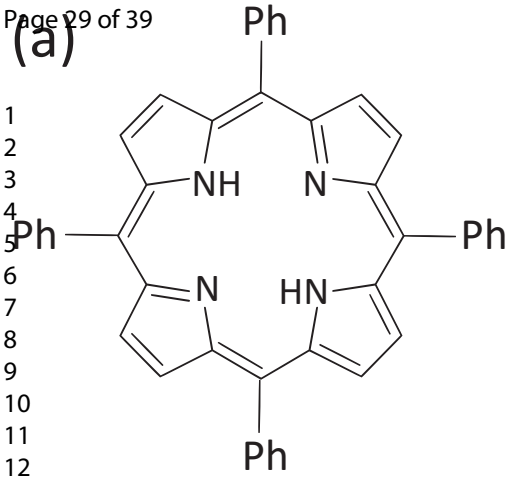

2H-TPP

(b)

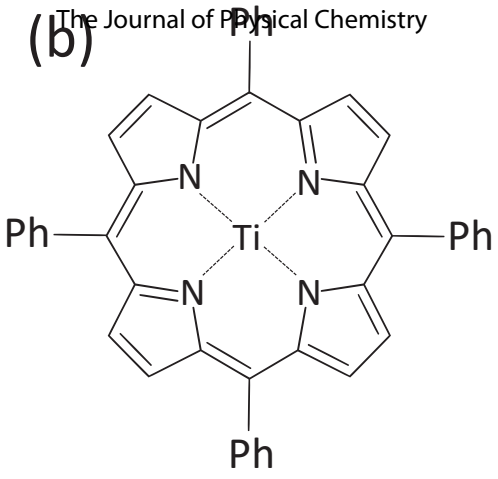

Ti-TPP

(c)

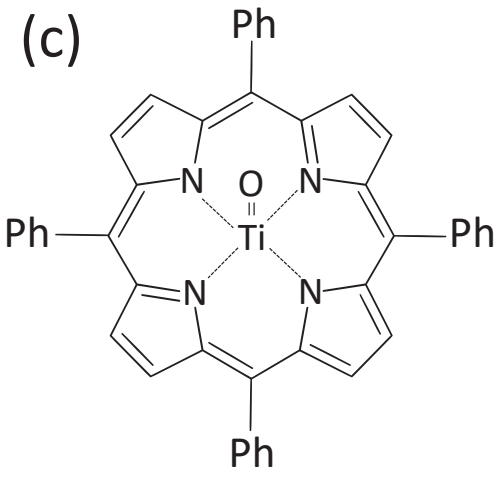

TiO-TPP

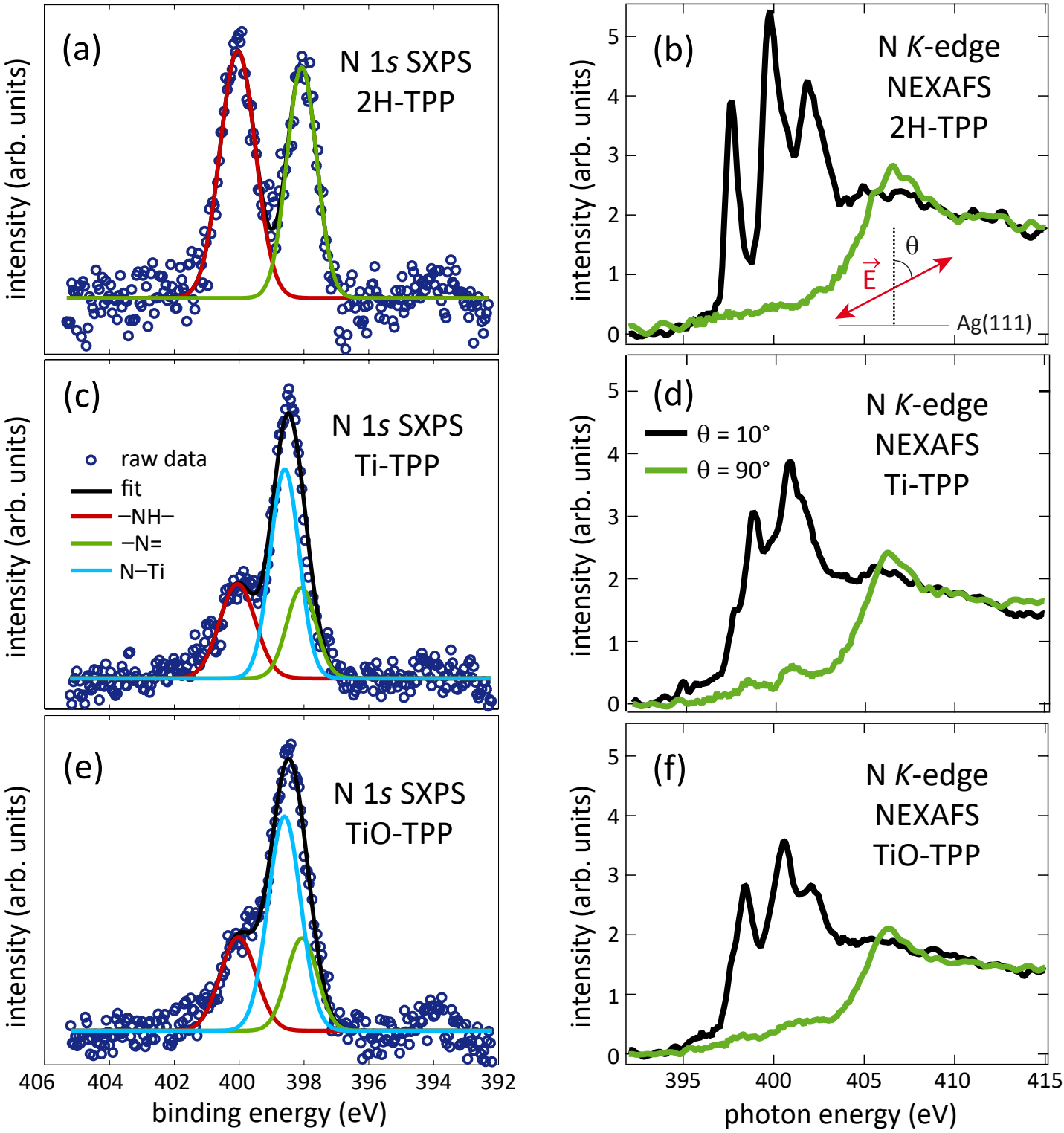
(a)
N 1s SXPS
2H-TPP
(b)
N K-edge
NEXAFS
2H-TPP
θ
E
Ag(111)
(c)
N 1s SXPS
Ti-TPP
raw data
fit
–NH–
–N=
N–Ti
(d)
N K-edge
NEXAFS
Ti-TPP
θ = 10°
θ = 90°
(e)
N 1s SXPS
TiO-TPP
(f)
N K-edge
NEXAFS
TiO-TPP
intensity (arb. units)
binding energy (eV)
photon energy (eV)
406
404
402
400
398
396
394
392
395
400
405
410
415
0
1
2
3
4
5

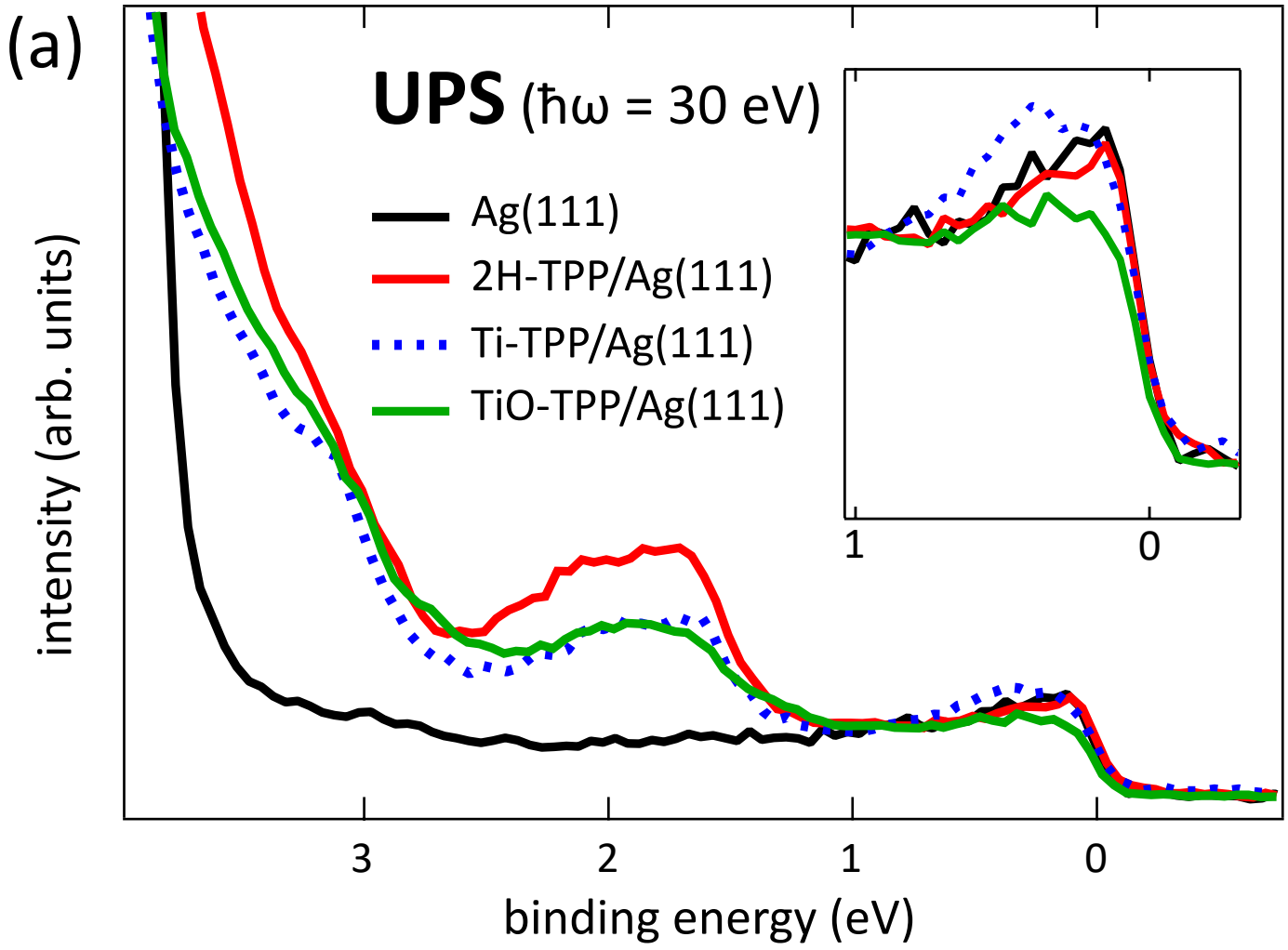
(a)
UPS (ħω = 30 eV)
Ag(111)
2H-TPP/Ag(111)
Ti-TPP/Ag(111)
TiO-TPP/Ag(111)
intensity (arb. units)
3
2
1
0
binding energy (eV)
1
0

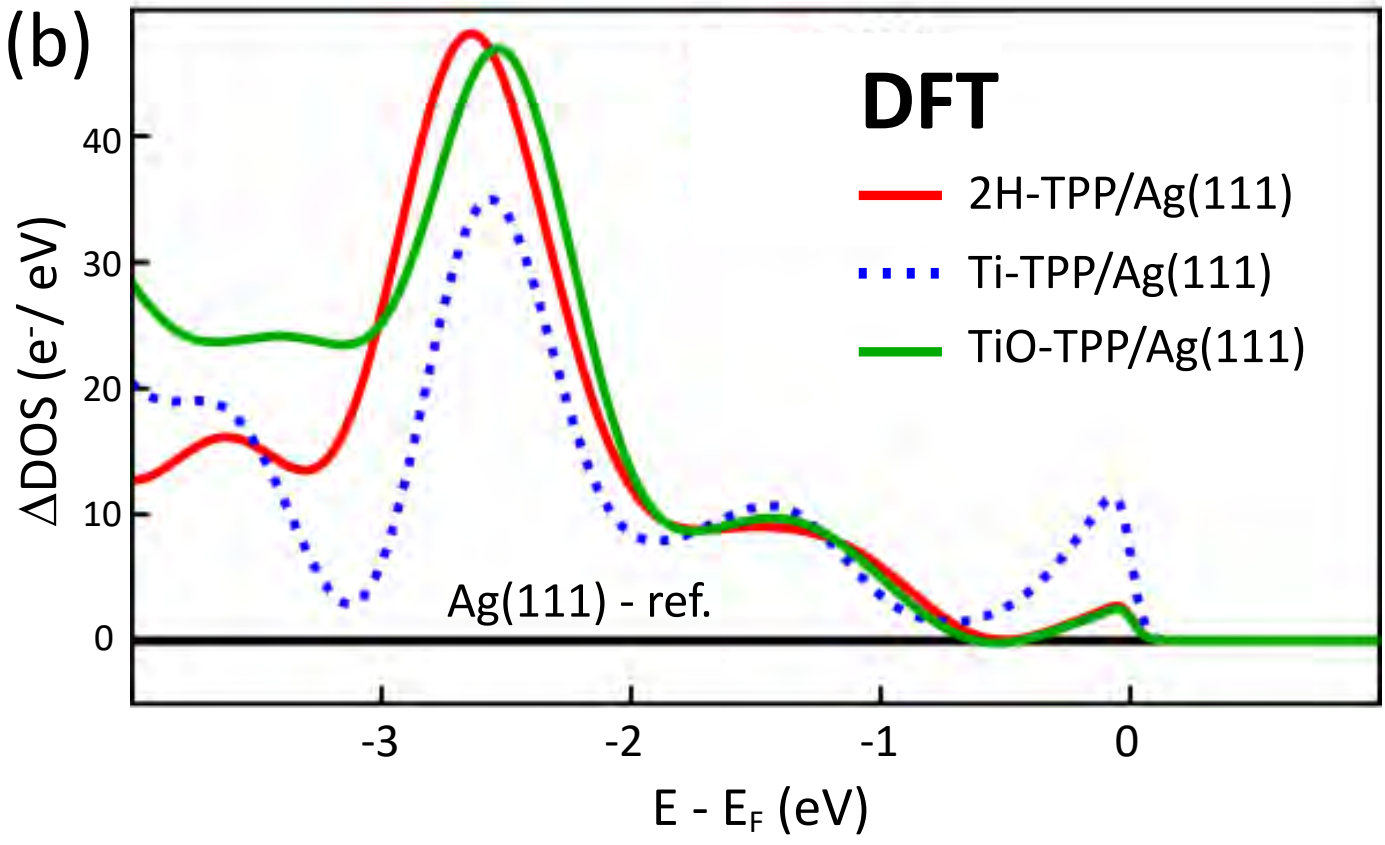
(b)
DFT
2H-TPP/Ag(111)
Ti-TPP/Ag(111)
TiO-TPP/Ag(111)
ΔDOS (e⁻/ eV)
40
30
20
10
0
Ag(111) - ref.
-3
-2
-1
0
E - E_F (eV)

(a) -1.0 V

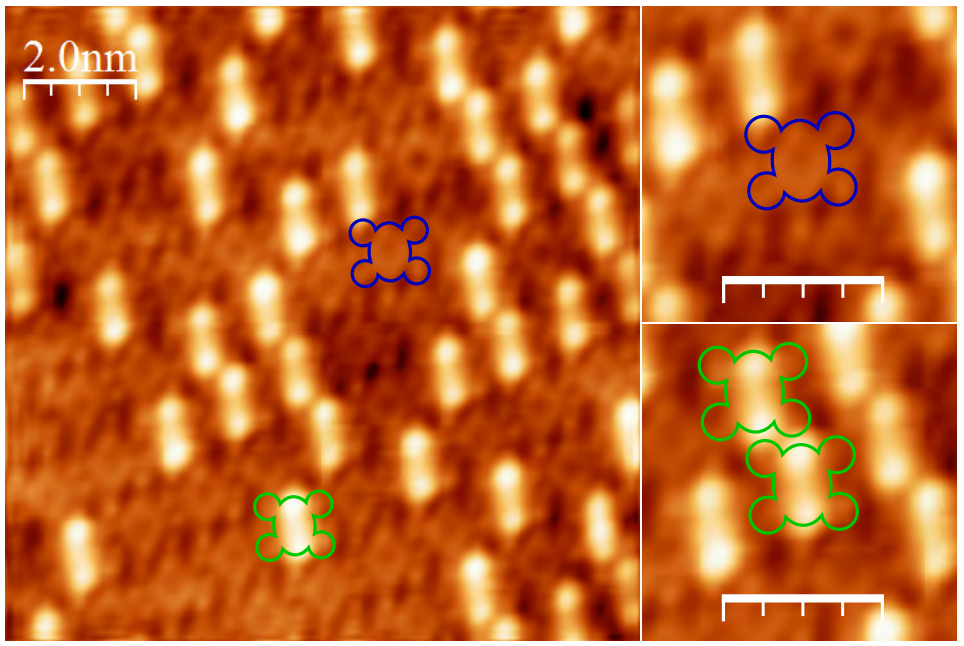

(b) +0.5 V

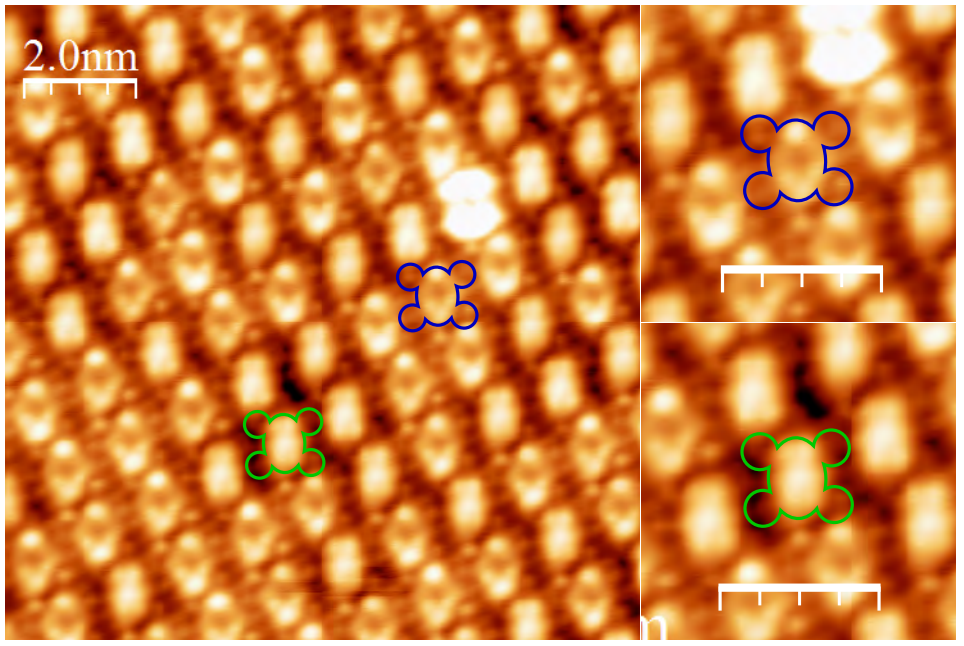

(c) -1.0 V

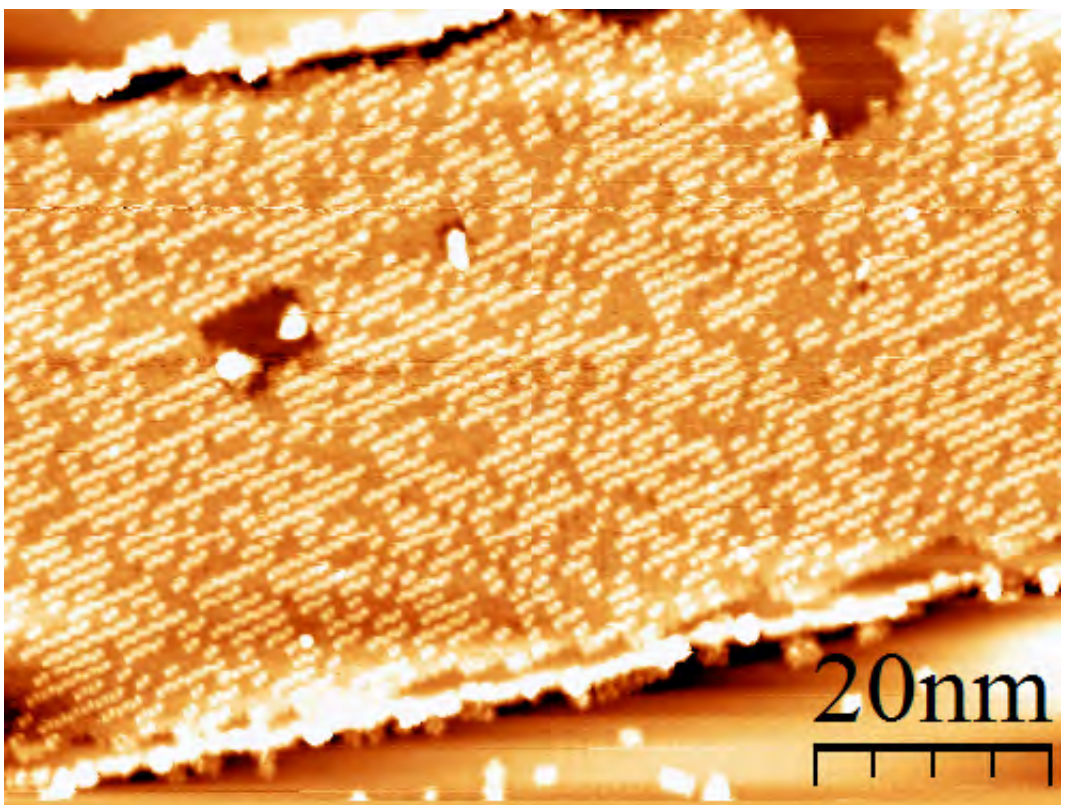

(d) -1.0 V

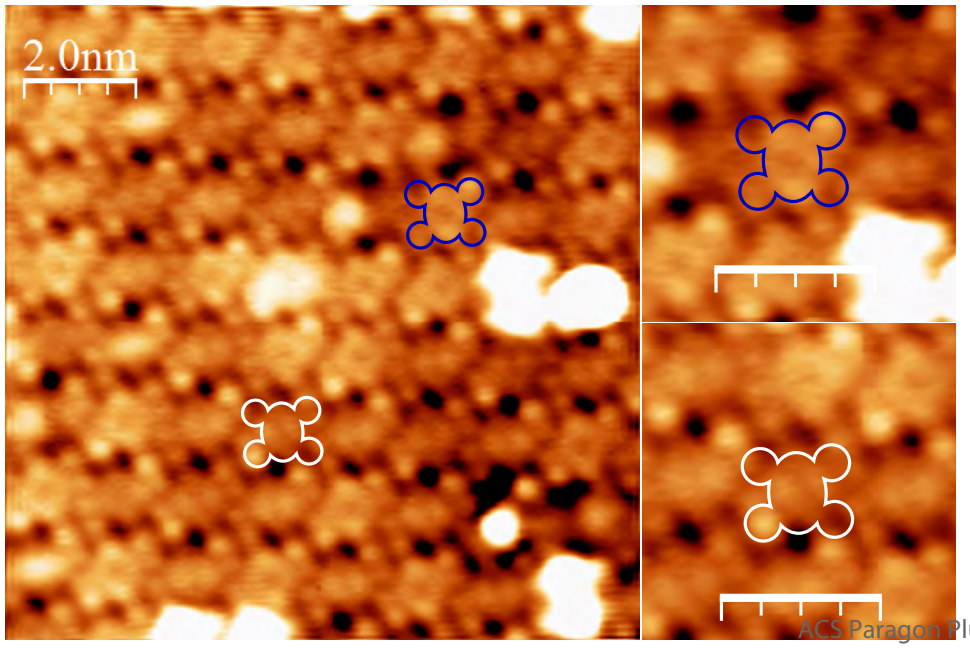

(e) +0.5 V

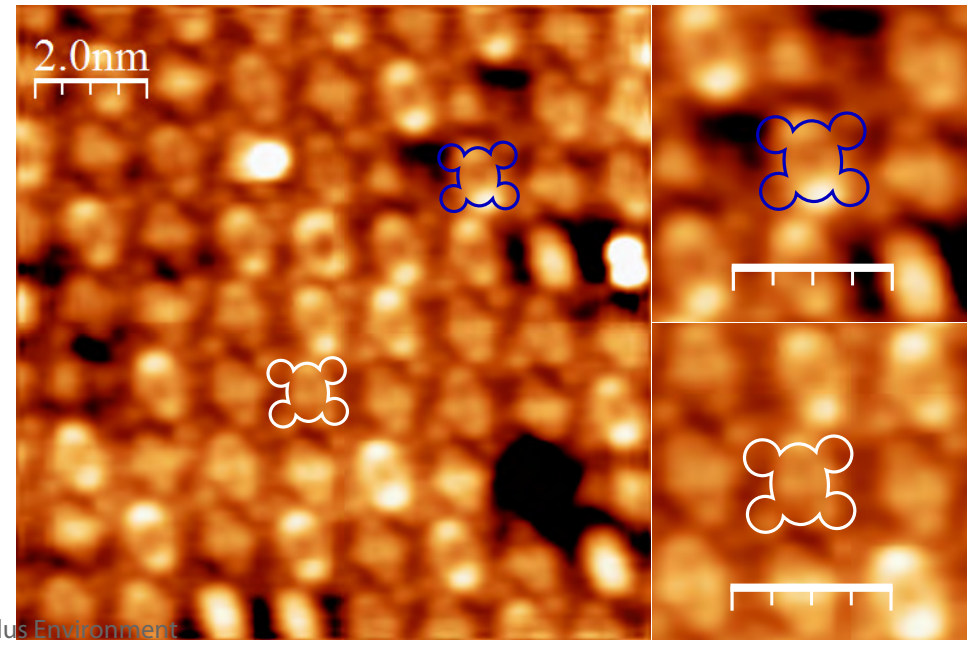

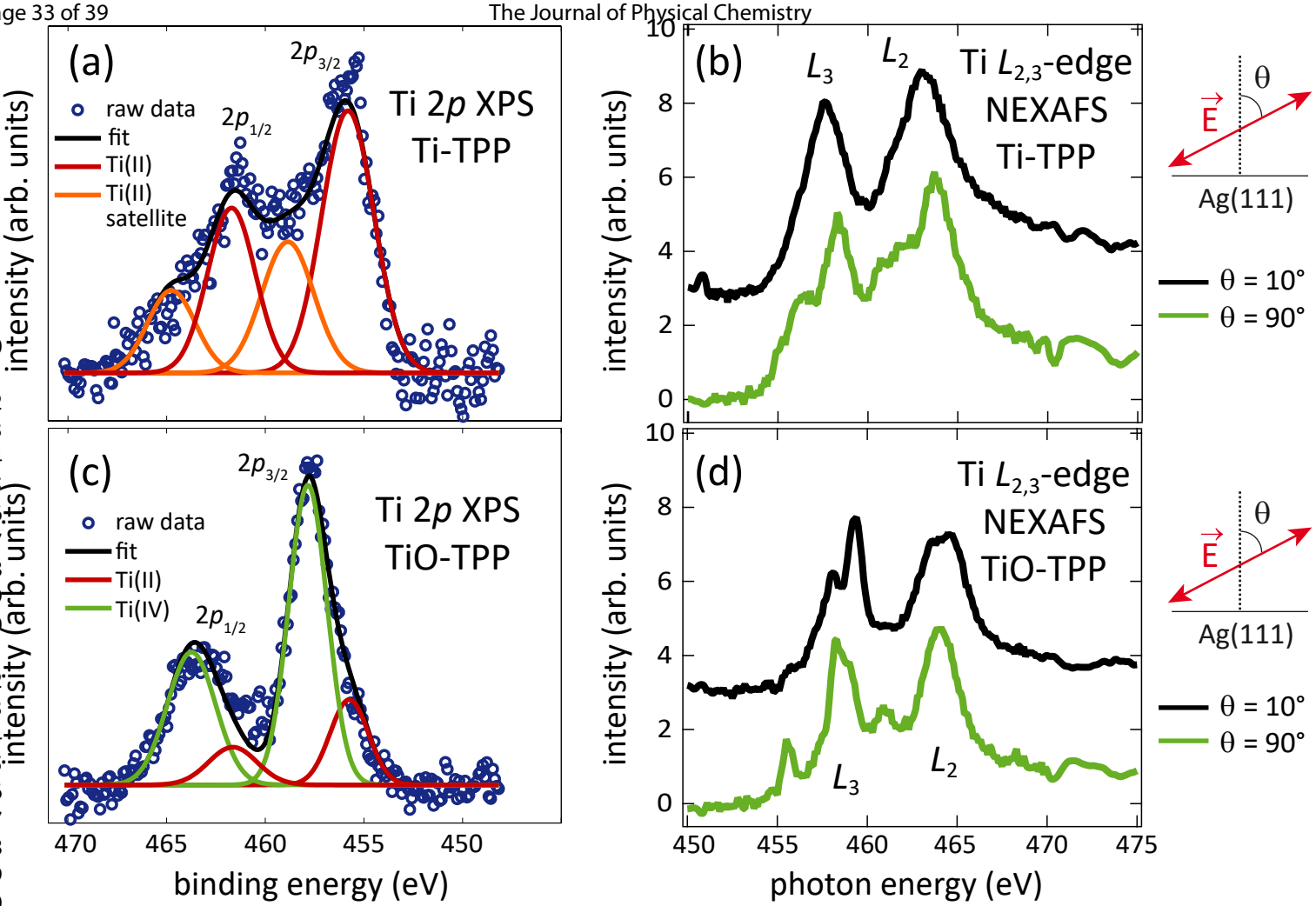
(a)
Ti 2p XPS
Ti-TPP
raw data
fit
Ti(II)
Ti(II) satellite
2p3/2
2p1/2
intensity (arb. units)
(b)
Ti L2,3-edge NEXAFS
Ti-TPP
L3
L2
θ
E
Ag(111)
θ = 10°
θ = 90°
(c)
Ti 2p XPS
TiO-TPP
raw data
fit
Ti(II)
Ti(IV)
2p3/2
2p1/2
(d)
Ti L2,3-edge NEXAFS
TiO-TPP
binding energy (eV)
photon energy (eV)

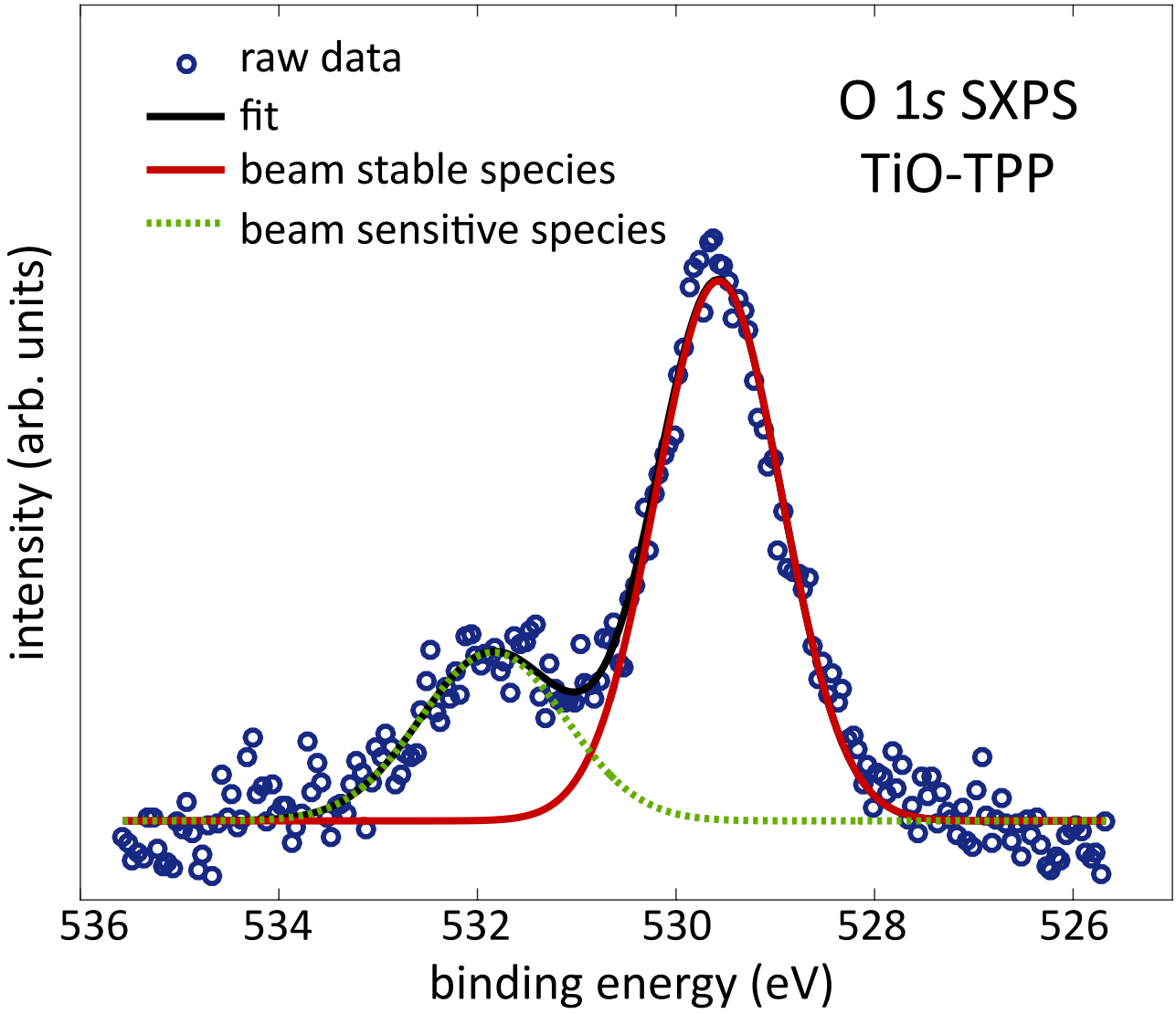
raw data
fit
beam stable species
beam sensitive species
O 1s SXPS
TiO-TPP
intensity (arb. units)
536
534
532
530
528
526
binding energy (eV)

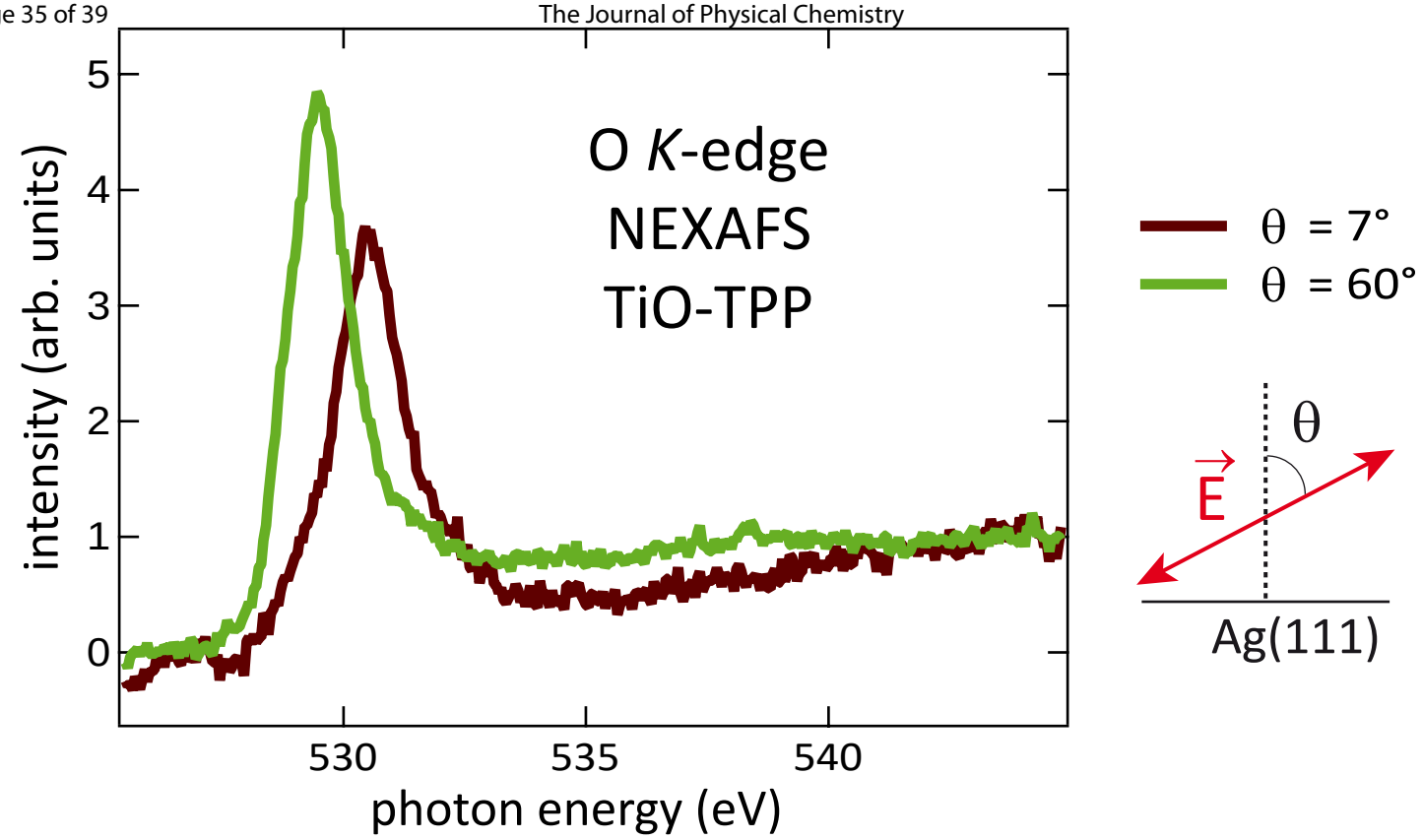
O K-edge
NEXAFS
TiO-TPP
intensity (arb. units)
photon energy (eV)
0
1
2
3
4
5
530
535
540
θ = 7°
θ = 60°
θ
E
Ag(111)

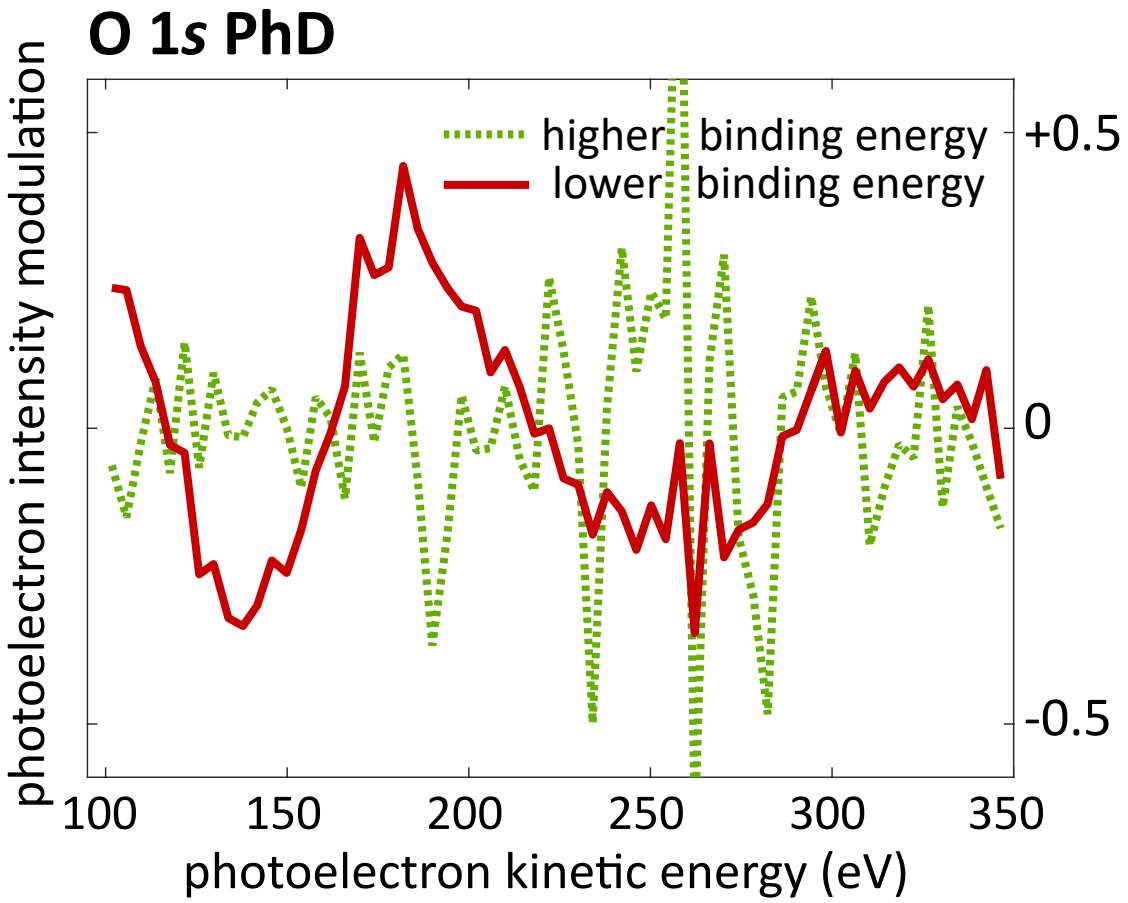
O 1s PhD
higher binding energy
lower binding energy
photoelectron intensity modulation
+0.5
0
-0.5
100
150
200
250
300
350
photoelectron kinetic energy (eV)

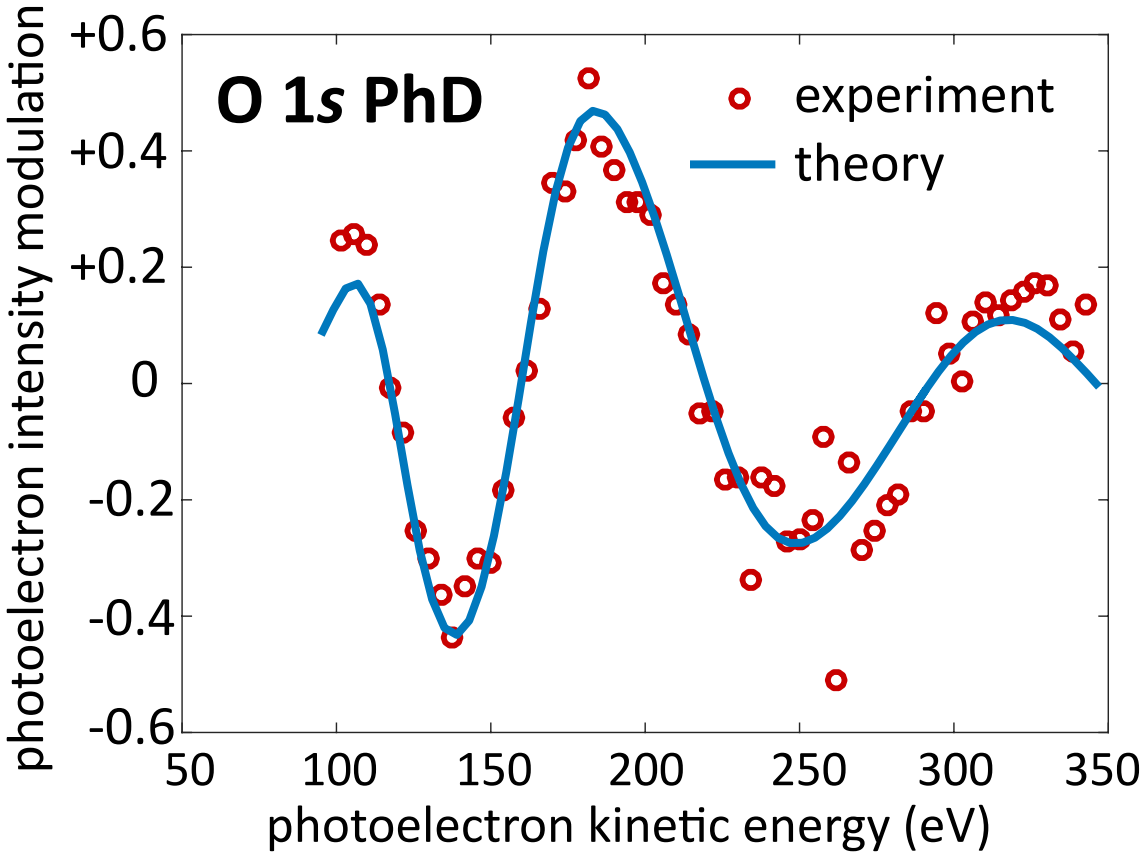
O 1s PhD
experiment
theory
photoelectron intensity modulation
+0.6
+0.4
+0.2
0
-0.2
-0.4
-0.6
50
100
150
200
250
300
350
photoelectron kinetic energy (eV)

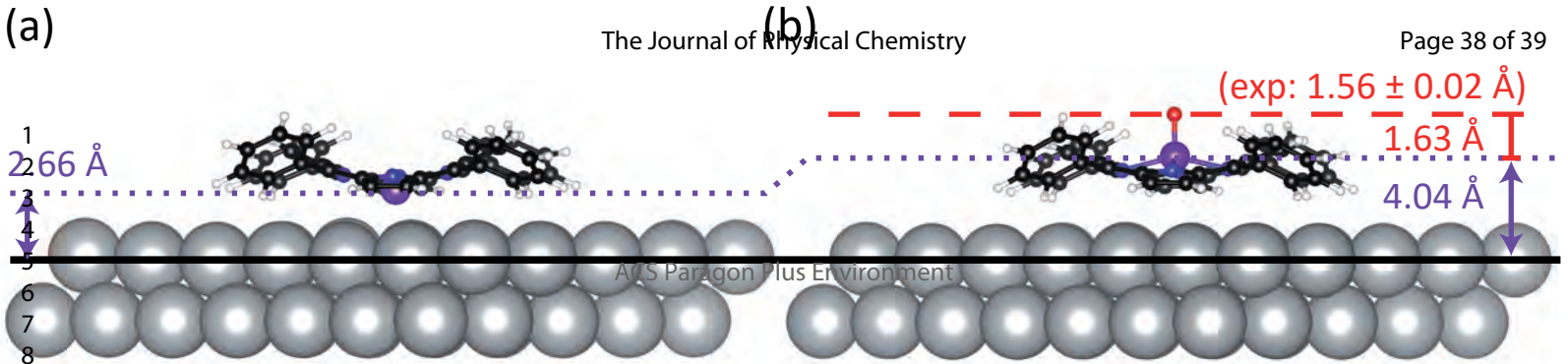
(a)
(b)
2.66 Å
(exp: 1.56 ± 0.02 Å)
1.63 Å
4.04 Å
ACS Paragon Plus Environment

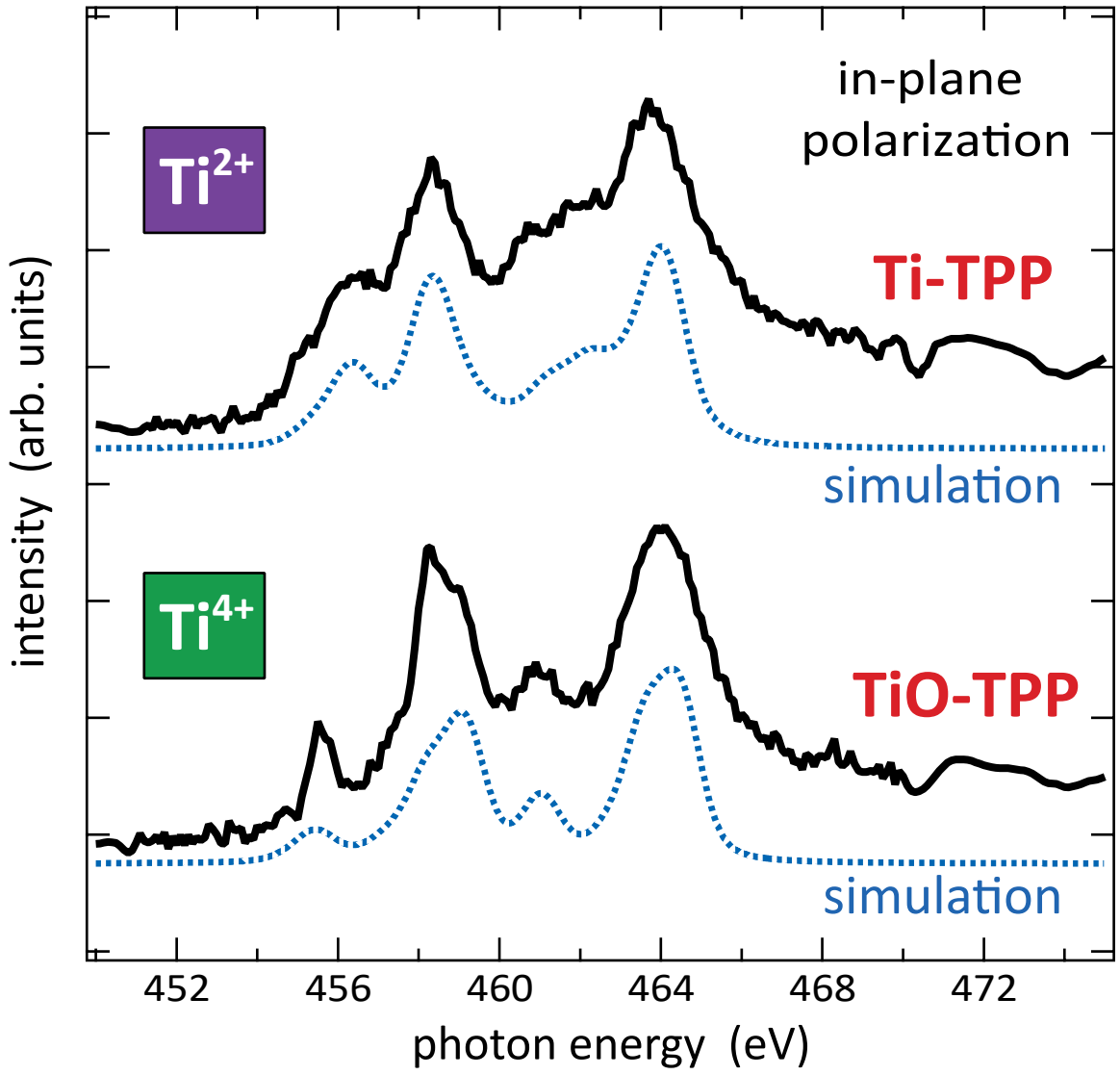
in-plane
polarization
Ti2+
Ti-TPP
simulation
Ti4+
TiO-TPP
simulation
intensity (arb. units)
452
456
460
464
468
472
photon energy (eV)